Received 26 March 2024; revised 23 April 2024; accepted 7 May 2024. Date of publication 13 May 2024; date of current version 31 May 2024.

Digital Object Identifier 10.1109/OJCOMS.2024.3400393

Multi-Connectivity Between Terrestrial and Non-Terrestrial MIMO Systems

BODONG SHANG [1] (Member, IEEE), XIANGYU LI [1,2], ZHUHANG LI [1], JUNCHAO MA [3] (Member, IEEE), XIAOLI CHU [4] (Senior Member, IEEE), AND PINGZHI FAN [5] (Fellow, IEEE)

[1] Eastern Institute for Advanced Study, Eastern Institute of Technology, Ningbo 315200, China

[2] Department of Electronic Engineering, Shanghai Jiao Tong University, Shanghai 200240, China

[3] School of Electrical and Information Engineering, Jiangsu University of Technology, Changzhou 213001, China

[4] Department of Electronic and Electrical Engineering, University of Sheffield, S1 3JD Sheffield, U.K.

[5] Key Laboratory of Information Coding and Transmission, Southwest Jiaotong University, Chengdu 610031, China

CORRESPONDING AUTHOR: B. SHANG (e-mail: bdshang@eitech.edu.cn)

This work was supported in part by the YongRiver Scientific and Technological Innovation Project under Grant 2023A-187-G.
The work of Pingzhi Fan was supported by NSFC under Project 62020106001.

ABSTRACT Communicating in a non-terrestrial network (NTN) has recently emerged as a promising technology to provide global seamless connectivity. Although low earth orbit (LEO) satellites in an NTN have been employed for providing ubiquitous coverage and high data rates for ground users, especially in emergent outdoor scenarios, NTN has not been integrated into the design of multi-connectivity for users in a terrestrial network (TN). Inspired by the 3rd Generation Partnership Program (3GPP) suggestion, this paper investigates TN-NTN-combined multi-connectivity downlink multiple-input multiple-output (MIMO) communication system, where each user may simultaneously connect to a base station (BS) in a TN and an LEO satellite in an NTN. Specifically, each user may have four different downlink access modes: served by both an LEO satellite and a BS, served by a BS, served by an LEO satellite, and not scheduled. Zero-forcing beamforming is employed at each LEO satellite to reduce the mutual interference among the satellite's served users, and maximum ratio transmission beamforming is used at each terrestrial BS to enhance the downlink signal strength. By deriving the probability of each access mode and modeling the interference in such a TN-NTN-combined multi-connectivity MIMO system, we obtain a typical user's downlink coverage probability and average achievable data rate. Extensive Monte Carlo simulations are conducted to validate our analytical derivations. Simulation results demonstrate that the user's coverage probability and average achievable data rate can be significantly improved by realizing multi-connectivity with both TN and NTN compared to pure TN or NTN.

INDEX TERMS Non-terrestrial network, LEO satellite communication, coverage probability, data rate, multi-connectivity, terrestrial network.

I. INTRODUCTION

THE MANAGEMENT of a growing number of users and requirements for higher coverage and data rate has been one of the bottlenecks for the development of communication networks [1]. The approach of deploying more low-power base stations (BSs), e.g., pico-cells, femto-cells and small-cells, though seems to be effective intuitively, will lead to the problem of complicated spectrum-sharing due to the nature of layered structure. Moreover, this approach may not be of enough sustainability considering the increasingly limited area on the ground level. The dense deployment of other emerging technologies, such as cell-free massive multiple-input multiple-output (MIMO), reconfigurable intelligent surfaces (RISs), and smart skins/repeaters, would entail higher costs for remote and rural areas.

Over the past years, the integration of terrestrial networks (TNs) and non-terrestrial networks (NTNs) has emerged as a promising avenue for advancing future communication

systems. This development has sparked significant interest from standardization bodies, network operators, research institutes, and related industries [2]. Notably, the 3rd Generation Partnership Program (3GPP) [3] is spearheading the evolution of a fifth-generation (5G) radio access network (RAN) for high availability and high reliability, incorporating NTN for multi-connectivity and link aggregation, as demonstrated in Release 15 [4] and Release 16 [5]. Further discussions on the standard protocol modifications are underway in Release 17 [6], [7]. This progress underscores the increasing need for research on TN-NTN-combined multi-connectivity for multi-cell networks on a global scale. Moreover, the imminent deployment of several LEO satellite projects, such as Kuiper, LeoSat, OneWeb, Starlink, and Telesat, aims to establish a comprehensive global communications network [8], [9].

For NTN, the geostationary earth orbit (GEO) satellites, located at an altitude of 35, 800 km, have been utilized for decades for the provision of mobile connectivity and broadcast services. Thanks to their fixed positions relative to the earth, they enjoy the advantages of comprehensive coverage and nearly constant latency [10]. However, it has been concluded in [11] that critical issues, such as high latency, significant free-space attenuation, and high latitudes with low elevation angles, no longer match the need for today's real-time and high-data-rate communications. Alternatively, low earth orbit (LEO) satellites have supported space-ground communications in recent years [12]. LEO satellite-supported communications, deployed at an altitude of as low as about 500 km, can reap the benefits of lower latency and path loss, thus, higher data rates with comparatively lower deployment cost. Some existing and representative LEO networks include OneWeb, LeoSat, Telesat, and SpaceX StarLink [13]. In this regard, LEO satellites can be considered as potential candidates for TN-NTN multi-connectivity scenarios.

MIMO [14] and massive MIMO [15] are key enabling technologies for 5G and beyond communication systems. By increasing the number of antennas and employing appropriate transmitting and receiving tactics, such as maximum ratio transmission (MRT), maximum ratio combining (MRC) and zero-forcing (ZF), and reasonable interference-reduction strategies, the system capacity can be significantly increased due to array gain, diversity gain, and spatial multiplexing gain [16]. Under this consideration, specific MIMO communication techniques will be likely to improve the communication efficiency and quality-of-service (QoS) of TN-NTN-combined multi-connectivity.

For analytical tractability and accuracy, stochastic geometry (SG) [17] has been extensively utilized as a powerful mathematical tool for the spatial analysis and evaluation of wireless networks in terms of coverage probability, desired and interfering signals, and other stochasticity-related indexes. Particularly, its wide applications have spread across popular scenarios such as unmanned aerial vehicle (UAV) networks [18], cognitive cellular networks [19], vehicular networks [20] etc. Following the inspirations from previous SG-based works, we develop a multi-connectivity MIMO communication system that leverages both TN and NTN and evaluate the coverage probability as well as the achievable data rate of the typical user.

A. RELATED WORK

Multi-connectivity technology has emerged as a promising solution to expand a user's connections from one to more, garnering significant interest from both academic and industry circles. In recent years, abundant researches on multi-connectivity focus mainly on TN. Related works [21], [22] explore multi-connectivity in millimeter-wave (mmWave) bands to increase the potential capacity for next-generation cellular systems. Another problem lies in the latency-reduction of multi-connectivity in TN to improve the QoS. In [23], multi-connectivity is a compelling enabler for ultra-reliable low-latency communications (URLLC). By applying dynamic control algorithms [24], the benefits of multi-connectivity can be reaped in device-to-device (D2D) cellular links [25], and multi-user scenarios [26]. Moreover, multi-connectivity has been widely explored in the upper layer of computer communications in terms of functional architecture design [27], flow-control forecasting [28], user-plane application [29] etc.

For NTN multi-connectivity, the authors in [30] have pointed out that using NTN can unlock its full potential to maximize communication efficiency. Unlike standardized multi-connectivity in TN, the realization of multi-connectivity in NTN is still undergoing a long way of exploration and facing several challenges. For example, the effectiveness of secondary node addition and traffic steering algorithms may severely influence users' experienced throughput [31]. Moreover, to increase the system capacity and the achievable data rate for users, many recent works have studied the integration of MIMO in satellite communications and satellite networks. Previous works, e.g., [32], [33], investigate the transmit designs for centralized massive MIMO (CMM) in LEO satellite communications with enough statistical channel state information (sCSI) and slow-varying sCSI. It has been shown that with adequately designed algorithms, MIMO is a promising approach to achieving significant performance gains. For distributed MIMO techniques in satellite networks, the authors of [2] and [34] explore the LEO satellite cooperation to support handheld devices using cross-layer design, artificial intelligence (AI)-based implementation, and broadband connectivity, showing superior performance compared to CMM modes. While satellite networks have shown significance in the QoS for ground users, this complete dependence on satellite works neglects potential communication services brought by TN. This has left room for research in the integrated networks formed by TN and NTN.

Further, for TN-NTN integration multi-connectivity, a measurement test [35] has been conducted to evaluate the performance of the LEO satellite network and the current cellular networks separately. It is shown that Starlink satellite

outperformed cellular networks in open areas; however, its potential for synergistic integration, i.e., a combined TN-NTN, needs to be studied. López et al. have completed empirical assessment [36] and analysis [37] in 5G terrestrial and LEO satellite networks. Although they reach the combination goal, they focus more on latency. The authors do not consider the actual coverage of the integrated TN-NTN, and throughput performance is only tested in a single-connectivity scenario. Moreover, theoretical analysis for TN-NTN has also been involved in [38]; actually, its emphasis lies in its designed dynamic activation algorithm for multi-connectivity, without a thorough and complete analysis of the structure of TN-NTN.

In [39], a multiple-access cell-free network where many IoT users are simultaneously served by a satellite in space and ground BSs is studied. However, it is challenging to implement the dense deployment of BSs on a large scale based on today's cellular networks, especially in rural and remote areas. Thus, there is a need to investigate the benefits of TN-NTN integrated systems for large-scale multi-cell networks. In addition, the influences of user scheduling on practical implementation remains unknown in its network. Reference [40] compares the LEO satellite-assisted communication system where ground gateways act as relays, with the BS-only system. It is pointed out that the coverage probability gains can be greatly increased with the use of LEO satellites, especially in rural and remote areas. In [41], the authors investigate an ultra-dense LEO satellite-terrestrial network, where terrestrial users are allowed to have access via LEO-assisted backhaul. It is shown that with a fixed number of LEO satellites, the proposed LEO satellite constellation achieves a coverage rate of at least 10% higher than that of the Telesat constellation. In addition, although there have been a few projects, such as 5G-ALLSTAR [42] and a geostationary satellite (GEO)-based field test [43], that explore and accelerate the progress of multi-connectivity development between TN and NTN, these implementations are only tested in limited space, while the realization in a global range is still left for the future [44].

It is worth noting that the researches mentioned above concentrated on either TN-supported or NTN-supported connectivity separately. At the same time, there has yet to be substantial progress in the research for integrated TN-NTN multi-connectivity, especially in global large-scale networks. This paper investigates an LEO satellite-supported multi-connectivity between TN and NTN systems for large-scale multi-cell networks.

We assume that users are randomly distributed on the ground based on users' random location. Moreover, we model the set of BSs as a Poisson point process (PPP) due to terrain constraints and the operator's deployment strategies. Since satellites move in various orbits, we model the set of satellites as another independent PPP on a spherical surface. To fully utilize channel capacity and improve efficiency, the system is modeled using the MIMO technique, employing different beamforming strategies at the multi-antenna downlink transmitters, i.e., satellites and terrestrial BSs. In addition, considering a user's chances of connection with the satellite, a probability model is built to analyze the coverage probability and data rate under four separate cases, i.e., Case 1 where a user is served by both TN and NTN, Case 2 where the user is only supported by TN, Case 3 where the user is only supported by NTN, and Case 4 where neither TN nor NTN provides connections. The four cases of our proposed integrated satellite-terrestrial networks offer various scenarios, especially in remote and rural areas. Here are some potential use cases for supporting the operation of "Case 1–3" with end-user devices equipped with both sub-6GHz patch antennas and satellite modules, i.e., integrated networks offer resilient communications in disaster-prone areas with damaged or nonexistent terrestrial infrastructure, ensuring reliable connectivity for emergency responders and affected communities [45]; in remote agricultural regions, they support precision agriculture techniques by enabling real-time monitoring and control of farming operations [46]; integrated networks also enhance connectivity along transportation routes, providing continuous communication links for vehicles and cargo containers.

B. PAPER CONTRIBUTIONS AND ORGANIZATION

The main contributions of our paper are summarized as follows:

- *Multi-Connectivity System Design:* We introduce a novel multi-connectivity MIMO communication system that allows a user to connect simultaneously to a BS in a TN and an LEO satellite in an NTN, where each user may have four different access modes, i.e., being served by both TN and NTN, being served by TN only, being served by NTN only, or not being scheduled. Specifically, when a user is served by both TN and NTN concurrently, it is connected to both a BS and an LEO satellite, forming a TN-NTN cooperative transmission system. The ZF beamforming (ZFBF) is used at each satellite to null the mutual interference among its served users, and the MRT beamforming (MRTBF) is employed at each BS to improve the downlink signal strength. To the best of the authors' knowledge, this is the first work that studies a mobile user's multi-connectivity with both TN and NTN while considering MIMO beamforming as well as multi-cell and large-scale interference.
- *Modeling and Analysis:* Based on the designed TN-NTN-combined multi-connectivity MIMO system, we derive the probability of each of the above four access modes for a typical user. In terms of problems in radio-resource sharing, inter-cell interference from TN occurs when a user is served by both TN and NTN, or by TN only; inter-satellite interference appears when it is served by both TN and NTN, or by NTN only; satellite-BS interference exists in the scenario when a user is served by both TN and NTN, or by TN only. In the TN-NTN combined multi-connectivity downlink MIMO

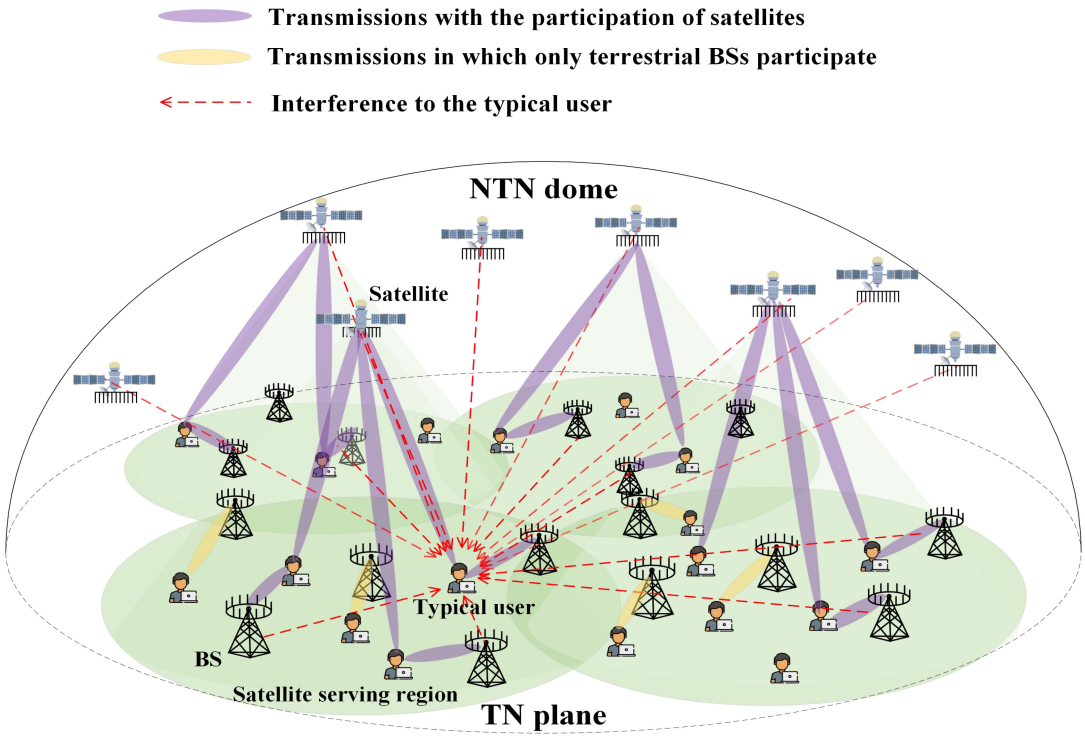

FIGURE 1. An illustration of multi-connectivity between TN and NTN MIMO systems.

system, we focus on scenarios in rural and remote areas, where trees and forests are often regarded as unavoidable obstructions. Therefore, line-of-sight (LoS) between terrestrial users and satellites can be blocked. The Shadowed-Rician fading is used to model the small-scale fading between satellites and terrestrial users, and we assume that the small-scale fading between a BS and a terrestrial user follows Rayleigh distribution. Furthermore, we characterize the coverage probability of a typical user in each access mode. Based on the four possible access modes, the downlink coverage probability and average achievable data rate of the typical user are derived.

- *System Design Insights:* The derived closed-form expressions are used to evaluate the performance of the designed system. Compared with the traditional TN single-connectivity and NTN single-connectivity schemes, the introduced TN and NTN multi-connectivity scheme improves the user's average achievable downlink data rate by over 100%. Therefore, integrating the satellite-terrestrial networks and allowing ground users' multi-connectivity with both satellites and ground BSs can significantly increase the user's downlink data rate. Moreover, when the number of satellite-served users is kept equal to the number of satellite antennas, increasing the number of satellite antennas improves the user's downlink data rate even with reduced satellite transmission power for the user.

The remainder of this paper is organized as follows. In Section II, the theoretical model of the multi-connectivity system between TN and NTN is elaborated, including BS-user and satellite-user channel models, downlink transmission process, and related performance metrics. Section III develops intermediate results to be used in derivations of both the coverage probability and the average achievable data rate. By dividing connection statuses into different cases, Section IV derives the coverage probability for a typical user. In Section V, simulation and numerical results are provided and analyzed. Finally, Section VI concludes the paper.

Notations: The operations of transpose, conjugate, conjugate transpose, and square are denoted by $(\cdot)^{\mathrm{T}}$, $(\cdot)^*$, $(\cdot)^{\mathrm{H}}$ and $|\cdot|^2$, respectively. The unitary space of dimensions $M \times N$ is represented as $\mathbb{C}^{M\times N}$. The symbols $\exp(\cdot)$ and $\emptyset$ denote exponential operations and the empty set, respectively. The ℓ_2-norm is denoted by $|\cdot|_2$. The statistical expectation and the probability are presented as $\mathbb{E}\{\cdot\}$ and $\mathbb{P}\{\cdot\}$, respectively.

II. SYSTEM MODEL

As shown in Fig. 1, we consider a multi-connectivity system that is composed of a TN and an NTN, with M_T-antenna BSs, M_N-antenna satellites, and single-antenna users. In the TN, BSs are distributed with a density of λ_T on the earth's surface following a homogeneous PPP. Users are distributed around each BS within the radius of R_T following a Poisson cluster process (PCP). The average number of users associated with a BS is denoted by U_T. In the NTN, we assume that the distribution of satellites follows a spherical PPP (SPPP) with the density of λ_N at the same orbital altitude. The serving region of each satellite is denoted by A_N with a radius of R_N and it is usually more than one BS situated in the serving

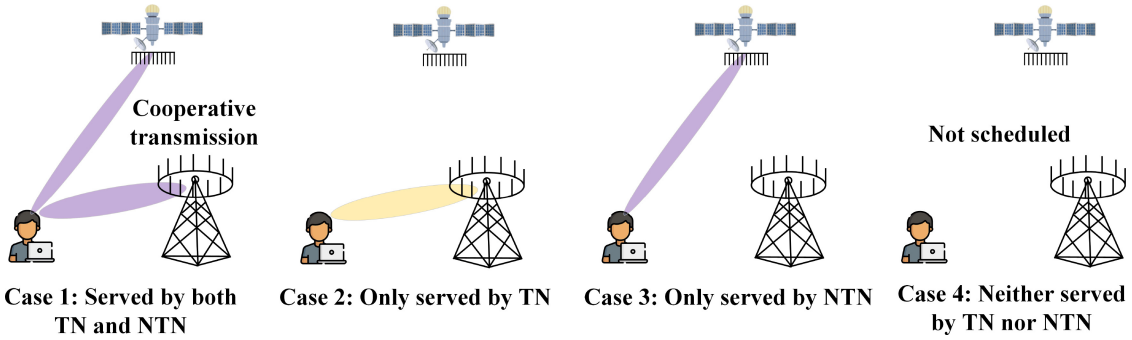

FIGURE 2. Four cases for a user's communication in TN and NTN multi-connectivity scheme.

region. It is assumed that the number of scheduled users of each satellite, i.e., K, does not exceed the number of antennas of the satellite, i.e., $K \leq M_N$, [32]. Moreover, the orbit altitude of satellites is H_N and the radius of the earth is R_E. The distance between a satellite and the center of the earth is $R_S = R_E + H_N$.

A. CHANNEL MODEL

1) BS-USER LINK

Rayleigh fading channels are utilized between BSs in TN and users. Let the channel between the j-th BS and the k-th user be $\mathbf{g}_{jk} = [g_{jk,1}, \ldots, g_{jk,M_T}]^{\mathrm{H}} \in \mathbb{C}^{M_T \times 1}$, where

$$g_{jk,m} = \sqrt{\beta_0^T l_{jk}^{-\alpha_T}} f_{jk,m}^T \tag{1}$$

is the channel from the m-th antenna of the j-th BS to the k-th user, β_0^T is the path-loss at a reference distance in TN, l_{jk} is the distance between the j-th BS and the k-th user, α_T denotes the path-loss exponent in BS-user links, $f_{jk,m}^T \in \mathbb{C}^{1\times 1}$ is the small-scale fading coefficient. The probability density function (PDF) of the fading power is given by

$$f_{\left|f_{jk,m}^T\right|^2}(x) = \lambda_0 \exp(-\lambda_0 x), \tag{2}$$

where $\lambda_0 = 1$ is the Rayleigh fading parameter.

2) SATELLITE-USER LINK

For channels between the satellites and the users, we consider that the channel fading in each link follows the Shadowed-Rician distribution. The channel between the i-th satellite and the k-th user is denoted by $\mathbf{h}_{ik} = [h_{ik,1}, \ldots, h_{ik,M_N}]^{\mathrm{H}} \in \mathbb{C}^{M_N \times 1}$, where

$$h_{ik,m} = \sqrt{\beta_0^N r_{ik}^{-\alpha_N}} f_{ik,m}^N \tag{3}$$

is the channel coefficient from the m-th antenna of the i-th satellite to the k-th user, β_0^N is the large-scale path-loss at a reference distance in NTN, r_{ik} is the distance between the i-th satellite and the k-th user, α_N denotes the path-loss exponent in satellite-user links, and $f_{ik,m}^N \in \mathbb{C}^{1\times 1}$ is the small-scale fading between the m-th antenna of the i-th satellite and the k-th user. According to [47], Nakagami parameter m_{Nak}, the average power of scattered component b_0, and the average power of LoS component Ω can be employed to represent the corresponding Shadowed-Rician (SR) fading characteristics. Since the square of a Nakagami random variable follows a Gamma distribution, we use a Gamma random variable to approximate the channel power gain of SR fading channel, i.e., $|f_{ik,m}^N|^2$, which can be represented as

$$f_{\left|f_{ik,m}^N\right|^2}(x) \approx \frac{1}{\beta^\kappa \Gamma(\kappa)} x^{\kappa-1} \exp\left(-\frac{x}{\beta}\right), \tag{4}$$

with κ denoted by [48], [49]

$$\kappa = \frac{m_{\mathrm{Nak}}(2b_0 + \Omega)^2}{4m_{\mathrm{Nak}}{b_0}^2 + 4m_{\mathrm{Nak}} b_0 \Omega + \Omega^2}, \tag{5}$$

and β denoted by

$$\beta = \frac{2b_0 + \Omega}{\kappa}, \tag{6}$$

where $\Gamma(\kappa)$ is the gamma function, while κ and β are parameters for the shape and scale of a Gamma distribution, respectively.[1]

B. DOWNLINK TRANSMISSION

As shown in Fig. 2, there are four cases for a user's communication in TN and NTN multi-connectivity scheme. In Case 1, the user is scheduled to be served by both a satellite and a BS for cooperative joint transmission in the same frequency band. When only one connection works, the user is served by either a BS in TN or a satellite in NTN, which is Case 2 and Case 3, respectively. Case 4 shows that the user is not scheduled in this system, where neither a BS nor a satellite provides service for the user in the current time slot. We follow the practical bandwidth configurations that satellite communication usually used, the Ka and Ku spectrum bands, denoted by $B_{1,3}$ for Case 1 and Case 3. The band for terrestrial BS communication is denoted by B_2 for Case 2. The total bandwidth is $B = B_{1,3} + B_2$, and we have $B_{1,3} \bigcap B_2 = \varnothing$.

[1] It is worth noting that we assume the perfect CSI knowledge at satellites and BSs [50], [51], [52], [53]. The derived coverage probability and data rate expressions give upper bound performance of the TN-NTN-combined multi-connectivity MIMO system.

We consider using ZFBF strategy with equal power allocation across the satellite beams to null interference from/to intra-satellite users, while the MRTBF strategy is utilized at terrestrial BSs to enhance the desired signal strength of the associated user with a pointing beam.[2] Considering complicated communication environment and random distributions of users and BSs, we consider equal power allocation for LEO satellites and BSs and round-robin scheduling for all users to obtain the basic outcomes as an average situation. It is worth noting that our model can be applied to different power allocation methods and user scheduling strategies. Advanced power control strategies and user scheduling policies can be designed to integrate this TN-NTN-combined multi-connectivity MIMO system.

In the following, we give the expressions of signal-to-interference-plus-noise ratio (SINR) at the typical user in each case.

1) CASE 1

In Case 1, the received signal at the typical user k is represented as

$$y_k = y_k^N + y_k^{T,\text{Case 1}} + z, \tag{7}$$

where y_k^N and $y_k^{T,\text{Case 1}}$ are the received signals at the k-th user from NTN and TN, respectively; z is the additive white Gaussian noise (AWGN) following the complex normal distribution.

For the received signal y_k^N at the k-th user, we have

$$\begin{aligned} y_k^N &= \sum_{k'} \mathbf{h}_{A(k')k}^{\mathrm{H}} \mathbf{w}_{k'} \sqrt{G_{A(k')}} \sqrt{P_{k'}^N} x_{k'} \\ &= \sum_{k' \in \Omega_{A(k)}^N} \mathbf{h}_{A(k)k}^{\mathrm{H}} \mathbf{w}_{k'} \sqrt{G_{ml}} \sqrt{P_{k'}^N} x_{k'} \\ &\quad + \sum_{k' \notin \Omega_{A(k)}^N} \mathbf{h}_{A(k')k}^{\mathrm{H}} \mathbf{w}_{k'} \sqrt{G_{sl}} \sqrt{P_{k'}^N} x_{k'} \\ &= \mathbf{h}_{A(k)k}^{\mathrm{H}} \mathbf{w}_k \sqrt{G_{ml}} \sqrt{P_k^N} x_k \\ &\quad + \sum_{i \in \Phi^N, i \neq A(k)} \sum_{k' \in \Omega_i^N} \mathbf{h}_{ik}^{\mathrm{H}} \mathbf{w}_{k'} \sqrt{G_{sl}} \sqrt{P_{k'}^N} x_{k'}, \end{aligned} \tag{8}$$

[2]Note that for both TN and NTN, the beamforming strategies are flexible, which include but not limited to ZFBF and MRTBF. This paper aims to use ZFBF and MRTBF separately for exploring the integration of different beamforming strategies under the TN-NTN framework. The extension to different combinations of beamforming strategies is left as future work.

where $A(k')$ denotes the k'-th user's serving satellite, and $\mathbf{w}_k$ is the normalized ZF transmit beamformer given by

$$\mathbf{w}_{k'} = \frac{\left(\mathbf{I}_{M_N} - \mathbf{H}_{-k'} \mathbf{H}_{-k'}^{\dagger}\right) \mathbf{h}_{A(k')k'}}{\left\| \left(\mathbf{I}_{M_N} - \mathbf{H}_{-k'} \mathbf{H}_{-k'}^{\dagger}\right) \mathbf{h}_{A(k')k'} \right\|_2}. \tag{9}$$

The channel matrices for the serving satellite of the k'-th user and its intra-cell users is given by $\mathbf{H}_{-k'} = [, \ldots, \mathbf{h}_{A(k')k}, \ldots,]_{k \neq k', k \in \Omega_{A(k')}^N}$, where $\Omega_{A(k')}^N$ denotes the served users of satellite $A(k')$ in a time slot, and $\mathbf{H}_{-k'}^{\dagger} = (\mathbf{H}_{-k'}^{\mathrm{H}} \mathbf{H}_{-k'})^{-1} \mathbf{H}_{-k'}^{\mathrm{H}}$. To consider the effects of satellite antenna gain, we denote $G_{A(k')}$ as the satellite antenna gain in NTN, where G_{ml} is the satellite antenna main-lobe gain and G_{sl} is the satellite antenna side-lobe gain. $P_{k'}^N$ is the satellite transmit power, and $x_{k'}$ is the normalized signal, intended for the k'-th user, with $\mathbb{E}\{|x_{k'}|^2\} = 1$.

For the received signal y_k^T from TN, we have

$$\begin{aligned} y_k^{T,\text{Case 1}} &= \sum_{j' \in \Phi^{T,\text{Case 1}}} \mathbf{g}_{j'k}^{\mathrm{H}} \mathbf{b}_{j'U(j')} \sqrt{P_{j'U(j')}^T} x_{U(j')} \\ &= \mathbf{g}_{jk}^{\mathrm{H}} \mathbf{b}_{jk} \sqrt{P_{jk}^T} x_k \\ &\quad + \sum_{j' \in \Phi^{T,\text{Case 1}}, j' \neq j} \mathbf{g}_{j'k}^{\mathrm{H}} \mathbf{b}_{j'U(j')} \sqrt{P_{j'U(j')}^T} x_{U(j')}, \end{aligned} \tag{11}$$

where $\Phi^{T,\text{Case 1}}$ is the set of BSs in TN working in Case 1 mode, $U(j')$ is the served user associated with the j'-th BS in a time slot, and $\mathbf{b}_{j'U(j')}$ is the normalized transmit beamformer at the j'-th BS for $U(j')$, which is given by $\mathbf{b}_{j'U(j')} = \frac{\mathbf{g}_{j'U(j')}}{\|\mathbf{g}_{j'U(j')}\|}$. Note that $\mathbf{b}_{j'U(j')}$ is the MRTBF which maximizes the received desired signal strength at user $U(j')$. $P_{j'U(j')}^T$ is the j-th BS's transmit power, and $x_{U(j')}$ is the normalized signal, both intended for $U(j')$. Based on the received signal in (7), the SINR at the typical user k in Case 1 is given by (10) at the bottom of the page. Note that the interference from other satellites and other BSs are considered in the derivation.

It's worth noting that this cooperative transmission between TN and NTN can be achieved by considering some practical implementation details. First, the synchronization between a TN BS and an NTN satellite need to be noticed. The locations of ground user, BS and satellite are known based on the global positioning system and the satellite's ephemeris. Therefore, the timing advance can be compensated in cooperative transmission between TN BS and NTN satellite, where the robust downlink synchronization performance can be achieved by the

$$\text{SINR}_k^{\text{Case 1}} = \frac{\left| \mathbf{h}_{A(k)k}^{\mathrm{H}} \mathbf{w}_k \sqrt{G_{ml}} \sqrt{P_k^N} x_k + \mathbf{g}_{jk}^{\mathrm{H}} \mathbf{b}_{jk} \sqrt{P_{jk}^T} x_k \right|^2}{\sum_{i \in \Phi^N, i \neq A(k)} \sum_{k' \in \Omega_i^N} \left| \mathbf{h}_{ik}^{\mathrm{H}} \mathbf{w}_{k'} \sqrt{G_{sl}} \sqrt{P_{k'}^N} x_{k'} \right|^2 + \sum_{j' \in \Phi^T, j' \neq j} \left| \mathbf{g}_{j'k}^{\mathrm{H}} \mathbf{b}_{j'U(j')} \sqrt{P_{j'U(j')}^T} x_{U(j')} \right|^2 + B_{1,3} {\sigma_{n_0}}^2}, \tag{10}$$

synchronization signal block (SSB) design in the multi-connectivity network [4], [5]. Second, the latency incurred by exchanging the information between TN and NTN needs to be noted. This can be addressed by considering the timing advance in TN and NTN. Third, it is worth noting that the signaling exchange for channel state information and transmitted signals needs to be implemented in the joint transmission. Thus, a trade-off exists between a system's performance gain and implementation complexity.

2) CASE 2

In Case 2, the user is only scheduled by a BS in TN, and the interference is only from other transmitting BSs. The received signal at the typical user k is expressed as

$$y_k = y_k^{T,\text{Case 2}} + z, \tag{12}$$

where $y_k^{T,\text{Case 2}}$ is shown in (11). The SINR at the typical user k in Case 2 is given by (13) at the bottom of the page.

3) CASE 3

In Case 3, the user is only scheduled by a satellite in NTN and the interference is from other satellites and the BSs that participate in Case 1's joint transmissions. The received signal at the typical user k is expressed as

$$y_k = y_k^{N} + y_k^{T,\text{Case 1}} + z, \tag{14}$$

where y_k^N is shown in (8) and $y_k^{T,\text{Case 1}}$ denotes the received signals from BSs in TN that participate in Case 1's joint transmission. The SINR at the typical user k in Case 3 is given by (15) at the bottom of the page, where the interference encompasses the interference from NTN and TN.

4) CASE 4

In Case 4, the typical user k is neither scheduled by a satellite nor by a BS in the current time slot. Thus, it is apparent that Case 4 can be regarded as a special case of Case 1 where both y_k^N and y_k^T from (7) appears to be zero. Then, the SINR at the typical user k in Case 4 can be directly shown as

$$\text{SINR}_k^{\text{Case 4}} = 0. \tag{16}$$

C. PERFORMANCE METRICS

By taking a summation of all conditioned cases, the total coverage probability of the designed TN-NTN combined multi-connectivity system is represented as

$$\begin{aligned}\mathbb{P}_{\text{cov}} = {} & \mathbb{P}\{\text{Case 1}\}\mathbb{P}\left\{\text{SINR}_k^{\text{Case 1}} \geq \gamma_{th} \middle| \text{Case 1}\right\} \\ & + \mathbb{P}\{\text{Case 2}\}\mathbb{P}\left\{\text{SINR}_k^{\text{Case 2}} \geq \gamma_{th} \middle| \text{Case 2}\right\} \\ & + \mathbb{P}\{\text{Case 3}\}\mathbb{P}\left\{\text{SINR}_k^{\text{Case 3}} \geq \gamma_{th} \middle| \text{Case 3}\right\}. \end{aligned} \tag{17}$$

Then, the achievable data rate at the typical user k is correspondingly given by

$$\begin{aligned} R = {} & \mathbb{P}\{\text{Case 1}\}B_{1,3}\mathbb{E}\left\{\log_2\left(1+\text{SINR}_k^{\text{Case 1}}\right)\middle|\text{Case 1}\right\} \\ & + \mathbb{P}\{\text{Case 2}\}B_2\mathbb{E}\left\{\log_2\left(1+\text{SINR}_k^{\text{Case 2}}\right)\middle|\text{Case 2}\right\} \\ & + \mathbb{P}\{\text{Case 3}\}B_{1,3}\mathbb{E}\left\{\log_2\left(1+\text{SINR}_k^{\text{Case 3}}\right)\middle|\text{Case 3}\right\}. \end{aligned} \tag{18}$$

According to the property of expectation, we have $\mathbb{E}\{X\} = \int_0^\infty \mathbb{P}\{X > x\}dx$ for $X > 0$, which brings

$$\begin{aligned}\mathbb{E}\left\{\log_2(1+\text{SINR}_k)\right\} &= \int_0^\infty \mathbb{P}\left\{\log_2(1+\text{SINR}_k) > t\right\}dt \\ &= \int_0^\infty \mathbb{P}\left\{\text{SINR}_k > 2^t - 1\right\}dt. \end{aligned} \tag{19}$$

The achievable data rate in (18) is written as

$$\begin{aligned} R = {} & \mathbb{P}\{\text{Case 1}\}B_{1,3}\int_0^\infty \mathbb{P}\left\{\text{SINR}_k^{\text{Case 1}} \geq 2^t - 1\right\}dt \\ & + \mathbb{P}\{\text{Case 2}\}B_2\int_0^\infty \mathbb{P}\left\{\text{SINR}_k^{\text{Case 2}} \geq 2^t - 1\right\}dt \\ & + \mathbb{P}\{\text{Case 3}\}B_{1,3}\int_0^\infty \mathbb{P}\left\{\text{SINR}_k^{\text{Case 3}} \geq 2^t - 1\right\}dt. \end{aligned} \tag{20}$$

The coverage probability in (17) characterizes the probability of a user's received SINR higher than a given threshold with the consideration of user's random location, the positions of satellites and BSs, fading variation, and scheduling. However, the average achievable data rate in (20) evaluates the ergodic data rate of a user that can achieve over time slots, fading, and network topology changes with different bandwidths for satellites and BSs communications.

$$\text{SINR}_k^{\text{Case 2}} = \frac{\left|\mathbf{g}_{jk}^{\text{H}}\mathbf{b}_{jk}\sqrt{P_{jk}^T}x_k\right|^2}{\sum_{j'\in\Phi^{T,\text{Case 2}},j'\neq j}\left|\mathbf{g}_{j'k}^{\text{H}}\mathbf{b}_{j'U(j')}\sqrt{P_{j'U(j')}^T}x_{U(j')}\right|^2 + B_2{\sigma_{n_0}}^2}, \tag{13}$$

$$\text{SINR}_k^{\text{Case 3}} = \frac{\left|\mathbf{h}_{A(k)k}^{\text{H}}\mathbf{w}_k\sqrt{G_{ml}}\sqrt{P_k^N}x_k\right|^2}{\sum_{i\in\Phi^N,i\neq A(k)}\sum_{k'\in\Omega_i^N}\left|\mathbf{h}_{ik}^{\text{H}}\mathbf{w}_{k'}\sqrt{G_{sl}}\sqrt{P_{k'}^N}x_{k'}\right|^2 + \sum_{j'\in\Phi^{T,\text{Case 1}}}\left|\mathbf{g}_{j'k}^{\text{H}}\mathbf{b}_{j'U(j')}\sqrt{P_{j'U(j')}^T}x_{U(j')}\right|^2 + B_{1,3}{\sigma_{n_0}}^2}, \tag{15}$$

III. INTERMEDIATE RESULTS

In this section, we will derive some intermediate technical results, i.e., related distributions, number of served users by TN and NTN, and the probability of connection for each of four cases, which will be used in the subsequent calculations of coverage probability and the achievable data rate.

A. RELATED DISTRIBUTION

Lemma 1: The PDF of the distance between the k-th user and its attached i-th satellite is given by

$$f_{r_{ik}}(r) = \frac{2r}{{R_N}^2}, H_N \le r \le \sqrt{{H_N}^2 + {R_N}^2} \tag{21}$$

where H_N is the orbit altitude of satellites, and R_N denotes the radius of satellite serving region.

Proof: For the circular serving region of a satellite, the PDF of distance from a user to the region center is

$$f_X(x) = \frac{2x}{{R_N}^2}, \tag{22}$$

for $0 \le x \le R_N$. The distance between the satellite and a user can be expressed as $Y = g(X) = \sqrt{X^2 + {R_N}^2}$, which brings $X = h_Y(y) = (Y^2 - {H_N}^2)^{\frac{1}{2}}$.

Taking its derivative over y, we obtain

$$\frac{dh_Y(y)}{dy} = y\left(y^2 - {H_N}^2\right)^{-\frac{1}{2}}. \tag{23}$$

Without loss of generality, the PDF of y, achieved by combining (22) and (23), is shown as follows [54]

$$f_Y(y) = \begin{cases} f_X(h_Y(y))\left|\frac{dh_Y(y)}{dy}\right|, H_N \le y \le \sqrt{{H_N}^2 + {R_N}^2} \\ 0, \quad \text{else} \end{cases} \tag{24}$$

where for $H_N \le y \le \sqrt{{H_N}^2 + {R_N}^2}$, $f_Y(y)$ can be further expressed as

$$\begin{aligned} f_Y(y) &= \frac{2\left(y^2 - {H_N}^2\right)^{\frac{1}{2}}}{{R_N}^2}\left|y\left(y^2 - {H_N}^2\right)^{-\frac{1}{2}}\right| \\ &= \frac{2y}{{R_N}^2}. \end{aligned} \tag{25}$$

Thus, the PDF of distance between the k-th user and its serving satellite, i.e., i-th satellite, is given by

$$f_{r_{ik}}(r) = \begin{cases} \frac{2r}{{R_N}^2}, H_N \le r \le \sqrt{{H_N}^2 + {R_N}^2} \\ 0, \quad \text{else} \end{cases} \tag{26}$$

which completes this proof. ■

Denote A_T as the serving area of a BS, i.e., $A_T = \pi {R_T}^2$. The PDF of the distance between the k-th scheduled user and its attached j-th BS, i.e., l_{jk}, is expressed as [55]

$$f_{l_{jk}}(l) = \frac{2l}{{R_T}^2}, 0 < l \le R_T, \tag{27}$$

where R_T is the radius of the BS's serving region. The average number of users associated with the j-th BS in TN, i.e., $\mathbb{E}\{\Omega_j^T\}$, is expressed as $\mathbb{E}\{|\Omega_j^T|\} = U_T$.

The number of users associated with the i-th satellite in NTN, i.e., $\mathbb{E}\{\Omega_i^N\}$, is given by

$$\begin{aligned} \mathbb{E}\left\{\left|\Omega_i^N\right|\right\} &\approx \sum_{n=0}^{\infty} n \frac{\left(\lambda_T \pi {R_N}^2 U_T\right)^n}{n!} e^{-\lambda_T \pi {R_N}^2 U_T} \\ &= \lambda_T \pi {R_N}^2 U_T. \end{aligned} \tag{28}$$

B. PROBABILITY OF CONNECTION

In this subsection, we provide the probabilities of the four cases respectively.

The probability of case 1 is given by

$$\mathbb{P}\{\text{Case 1}\} = \frac{K}{\mathbb{E}\left\{\Omega_i^N\right\}} \frac{1}{\mathbb{E}\left\{\Omega_i^T\right\}}, \tag{29}$$

where we assume that there is at least one BS in the serving area of a satellite A_N, and $\mathbb{E}\{\Omega_i^N\}$ is given in (28).

The probability of case 2 is given by

$$\mathbb{P}\{\text{Case 2}\} = \left(1 - \frac{K}{\mathbb{E}\left\{\Omega_i^N\right\}}\right) \frac{1}{\mathbb{E}\left\{\Omega_i^T\right\}}. \tag{30}$$

The probability of case 3 is given by

$$\mathbb{P}\{\text{Case 3}\} = \frac{K}{\mathbb{E}\left\{\Omega_i^N\right\}} \left(1 - \frac{1}{\mathbb{E}\left\{\Omega_i^T\right\}}\right). \tag{31}$$

The probability of case 4 is given by

$$\mathbb{P}\{\text{Case 4}\} = \left(1 - \frac{K}{\mathbb{E}\left\{\Omega_i^N\right\}}\right) \left(1 - \frac{1}{\mathbb{E}\left\{\Omega_i^T\right\}}\right). \tag{32}$$

It is worth noting that the summation of (29), (30), (31), and (32) equals to one. The above probabilities of different cases will be used to calculate the system overall performance, such as (17) and (20). In the next Section, we will derive the coverage probability under each case.

IV. PERFORMANCE ANALYSIS

Denote the following terms which will appear in the subsequent analysis. Specifically, DS_k^N in (36) represents the desired signal power at the typical user k from NTN. DS_k^T in (34) indicates the desired signal power at the user k from TN. I_k^N in (35) is the interference power at the user k generated from NTN. I_k^T in (36) denotes the interference power at the user k generated from TN.

$$DS_k^N = \left|\mathbf{h}_{A(k)k}^{\mathrm{H}} \mathbf{w}_k \sqrt{G_{ml}} \sqrt{P_k^N} x_k\right|^2, \tag{33}$$

$$DS_k^T = \left|\mathbf{g}_{jk}^{\mathrm{H}} \mathbf{b}_{jk} \sqrt{P_{jk}^T} x_k\right|^2, \tag{34}$$

$$I_k^N = \sum_{i \in \Phi^N, i \ne A(k)} \sum_{k' \in \Omega_i^N} \left|\mathbf{h}_{ik}^{\mathrm{H}} \mathbf{w}_{k'} \sqrt{G_{sl}} \sqrt{P_{k'}^N} x_{k'}\right|^2, \tag{35}$$

$$I_k^{T,\text{Case 1/2}} = \sum_{j' \in \Phi^{T,\text{Case 1/2}}, j' \ne j} \left|\mathbf{g}_{j'k}^{\mathrm{H}} \mathbf{b}_{j'U(j')} \sqrt{P_{j'U(j')}^T} x_{U(j')}\right|^2. \tag{36}$$

In TN, when a user is served by its nearest BS, the distance l should be smaller than the radius of BS's serving area, i.e.,

$0 < l < R_T$ as shown in (27). For interference signal from TN, we also set a minimum interfering distance $r^T_{I,\min}$ that equals to l.

In NTN, as the radius of satellite serving region is defined as R_N, the lower and upper integral limits of the desired signal are $r^N_{DS,\min} = H_N$ and $r^N_{DS,\max} = \sqrt{{R_N}^2 + {H_N}^2}$, while those of the interference power are $r^N_{I,\min} = r_{ik}$ which is the distance from the typical user to its nearest serving satellite, and $r^N_{I,\max} = \sqrt{{R_S}^2 - {R_E}^2}$ which represents the distance between a satellite and its point of tangency with the earth, i.e., length of the tangent line, respectively.

A. CASE 1

The coverage probability conditioned on Case 1 is derived in (37) at the bottom of the page, where the interference power from satellites in NTN, and that from BSs in TN in Case 1 is given by I^N_k and $I^{T,\text{Case 1}}_k$, respectively.

Since the Shadowed-Rician fading channel between the satellite and the user can be approximated by a Gamma distribution, we have $|f^N_{A(k)k}|^2 \sim \Gamma(\kappa, \beta)$, where $\Gamma(\kappa, \beta)$ is the gamma function with shape κ and scale β. The sum of independent Gamma random variables can be approximated as a single Gamma random variable with appropriate shape and scale parameters [56]. The channel power of the intended signal for the typical user k in NTN is represented as

$$\left\|\mathbf{h}^{\mathrm{H}}_{ik}\right\|^2 = \sum_{m=1}^{M_N} \beta^N_0 {r_{ik}}^{-\alpha_N} f^N_{ik} \left(f^N_{ik}\right)^{\mathrm{H}}, \tag{42}$$

which follows a Gamma distribution, i.e., $\|\mathbf{h}^{\mathrm{H}}_{ik}\|^2 \sim \Gamma(M_N\kappa, \beta^N_0 {r_{ik}}^{-\alpha_N}\beta)$.

According to the property of Gamma distribution, $X \sim \Gamma(k, \theta)$ brings about $CX \sim \Gamma(k, C\theta)$. By projecting the channel vector onto the ZF beamformer [57], we obtain

$$\left|\mathbf{h}^{\mathrm{H}}_{ik}\mathbf{w}_k\right|^2 \sim \Gamma\Big((M_N - K + 1)\kappa, \beta^N_0 {r_{ik}}^{-\alpha_N}\beta\Big). \tag{43}$$

Then, we have

$$\left|\mathbf{h}^{\mathrm{H}}_{ik}\mathbf{w}_k\right|^2 \approx \beta\beta^N_0 {r_{ik}}^{-\alpha_N} \Lambda^N_{DS,k}, \tag{44}$$

where $\Lambda^N_{DS,k} \sim \Gamma((M_N - K + 1)\kappa, 1)$.

Taking $Y = DS^N_k + DS^T_k$, we rewrite (37) as

$$\begin{aligned}&\mathbb{P}\Big\{\mathrm{SINR}^{\text{Case 1}}_k \geq \gamma_{th}\Big\}\\ &\quad\geq \mathbb{P}\Big\{Y \geq \gamma_{th}\Big(I^N_k + I^{T,\text{Case 1}}_k + B_{1,3}{\sigma_{n_0}}^2\Big)\Big\},\end{aligned} \tag{45}$$

$$\begin{aligned}&\mathbb{P}\Big\{\mathrm{SINR}^{\text{Case 1}}_k \geq \gamma_{th}\Big|\text{Case 1}\Big\}\\ &= \mathbb{P}\left\{\frac{\left|\mathbf{h}^{\mathrm{H}}_{A(k)k}\mathbf{w}_k\sqrt{G_{ml}}\sqrt{P^N_k}x_k + \mathbf{g}^{\mathrm{H}}_{jk}\mathbf{b}_{jk}\sqrt{P^T_{jk}}x_k\right|^2}{I^N_k + I^{T,\text{Case 1}}_k + B_{1,3}{\sigma_{n_0}}^2} \geq \gamma_{th}\right\}\\ &= \mathbb{P}\left\{\left|\mathbf{h}^{\mathrm{H}}_{A(k)k}\mathbf{w}_k\sqrt{G_{ml}}\sqrt{P^N_k}x_k + \sum_{j\in\Phi^T_k}\mathbf{g}^{\mathrm{H}}_{jk}\mathbf{b}_{jk}\sqrt{P^T_{jk}}x_k\right|^2 \geq \gamma_{th}\Big(I^N_k + I^{T,\text{Case 1}}_k + B_{1,3}{\sigma_{n_0}}^2\Big)\right\}\\ &\geq \mathbb{P}\Big\{DS^N_k + DS^T_k \geq \gamma_{th}\Big(I^N_k + I^{T,\text{Case 1}}_k + B_{1,3}{\sigma_{n_0}}^2\Big)\Big\}.\end{aligned} \tag{37}$$

$$\psi(r,l) = \frac{\mu^2}{(M_N - K + 1)\kappa\left(\frac{G_{ml}P_N}{\mathbb{E}\{|\Omega^N_i|\}}\beta\beta^N_0 {r_{ik}}^{-\alpha_N}\right)^2 + M_T\left(P_T\beta^T_0 {l_{jk}}^{-\alpha_T}\right)^2}, \tag{38}$$

$$\zeta(r,l) = \frac{(M_N - K + 1)\kappa\left(\frac{G_{ml}P_N}{\mathbb{E}\{|\Omega^N_i|\}}\beta\beta^N_0 {r_{ik}}^{-\alpha_N}\right)^2 + M_T\left(P_T\beta^T_0 {l_{jk}}^{-\alpha_T}\right)^2}{\mu}, \tag{39}$$

$$\mu = (M_N - K + 1)\kappa\frac{G_{ml}P_N}{\mathbb{E}\{|\Omega^N_i|\}}\beta\beta^N_0 {r_{ik}}^{-\alpha_N} + M_T P_T\beta^T_0 {l_{jk}}^{-\alpha_T}. \tag{40}$$

$$\mathbb{P}\Big\{\mathrm{SINR}^{\text{Case 1}}_k \geq \gamma_{th}\Big|\text{Case 1}\Big\} \geq 1 - \mathbb{E}\left\{\frac{1}{\Gamma(\psi(r,l))}\gamma\left(\psi(r,l), \frac{\gamma_{th}\Big(I^N_k + I^{T,\text{Case 1}}_k + B_{1,3}{\sigma_{n_0}}^2\Big)}{\zeta(r,l)}\right)\right\}. \tag{41}$$

and we have

$$DS_k^N \sim \Gamma\left((M_N - K + 1)\kappa, \frac{G_{ml}P_N}{\mathbb{E}\{|\Omega_i^N|\}}\beta\beta_0^N r_{ik}{}^{-\alpha_N}\right), \quad (46)$$

$$DS_k^T \sim \Gamma\left(M_T, P_T\beta_0^T l_{jk}{}^{-\alpha_T}\right). \quad (47)$$

Note that Y can be approximated by a Gamma random variable, i.e., $Y \sim \Gamma(\psi, \zeta)$, based on the Welch-Satterthwaite approximation [58]. Following this approximation, we denote the PDF of Y as

$$f_Y(y) \approx \frac{1}{\Gamma(\psi)\zeta^\psi} y^{\psi-1} e^{-\frac{y}{\zeta}}, \quad (48)$$

where ψ and ζ are shown in (38) and (39), respectively, at the bottom of the previous page. The cumulative distribution function (CDF) of Y is approximated by

$$F_Y(y) \approx \frac{1}{\Gamma(\psi)}\gamma\left(\psi, \frac{y}{\zeta}\right), \quad (49)$$

where $\gamma(\cdot,\cdot)$ is the lower incomplete gamma function. Then, the complementary CDF (CCDF) of Y is

$$\mathbb{P}\{Y \geq y\} \approx 1 - \frac{1}{\Gamma(\psi)}\gamma\left(\psi, \frac{y}{\zeta}\right). \quad (50)$$

According to (50), the coverage probability can be initially written as (41) at the bottom of the previous page. For the interference power generated from satellites in NTN, we have

$$\left|\mathbf{h}_{A(k')k}^{\mathrm{H}}\mathbf{w}_{k'}\right|^2 \approx \beta_0^N r_{A(k')k}{}^{-\alpha_N}\Lambda_{I,A(k')k}^N, \quad (52)$$

where $\Lambda_{I,A(k')k}^N$ follows an exponential distribution, i.e., $\Lambda_{I,A(k')k}^N \sim \exp(1)$, due to the ZFBF and its projection on other channel vectors. The average interference power from satellites where the equal power allocation at each satellite is considered, equivalently denoted as $\Upsilon_N^{\text{Case 1}}(r)$, is

$$\begin{aligned}
\Upsilon_N^{\text{Case 1}}(r) &= \mathbb{E}\left\{I_k^N\right\} \\
&= \mathbb{E}\left\{\sum_{i'\in\Phi^N, i'\neq i}\sum_{k'\in\Omega_{i'}^N}\left|\mathbf{h}_{ik}^{\mathrm{H}}\mathbf{w}_{k'}\sqrt{P_{k'}^N}x_{k'}\right|^2\right\} \\
&= \mathbb{E}\left\{\frac{G_{sl}P_N}{\mathbb{E}\{|\Omega_i^N|\}}\beta\beta_0^N\sum_{i'\in\Phi^N, i'\neq i}\sum_{k'\in\Omega_{i'}^N}\Lambda_{I,i'k}^N r_{i'k}{}^{-\alpha_N}\right\} \\
&= \mathbb{E}\left\{G_{sl}P_N\beta\beta_0^N\sum_{i'\in\Phi^N, i'\neq i}\Lambda_{I,i'k}^N r_{i'k}{}^{-\alpha_N}\right\} \\
&= \mathbb{E}\left\{G_{sl}P_N\beta\beta_0^N\sum_{i'\in\Phi^N, i'\neq i}\mathbb{E}\left\{\Lambda_{I,i'k}^N\right\} r_{i'k}{}^{-\alpha_N}\right\} \\
&\overset{(a)}{=} G_{sl}P_N\beta\beta_0^N 2\pi\lambda_N\frac{R_N}{R_T}\int_{r_{ik}}^{r_{I,\max}^N} v^{-\alpha_N+1}dv \\
&\overset{(b)}{=} G_{sl}P_N\beta\beta_0^N\frac{2\pi}{\alpha_N-2}\frac{R_N}{R_T}\lambda_N\left(r^{2-\alpha_N} - r_{I,\max}^N{}^{2-\alpha_N}\right), \quad (53)
\end{aligned}$$

where (a) follows from $\mathbb{E}\{\Lambda_{I,i'k}^N\} = 1$ and Campbell's theorem of the SPPP, while (b) is obtained by

$$\int_{r_{ik}}^{r_{I,\max}^N} v^{-\alpha_N+1}dv = \frac{1}{\alpha_N-2}\left(r^{2-\alpha_N} - r_{I,\max}^N{}^{2-\alpha_N}\right). \quad (54)$$

Since some BSs participate in the joint transmission with satellites in frequency band $B_{1,3}$, the density of interfering BSs in Case 1 is given by $\lambda_{TN} = \frac{\mathbb{E}\{|\Omega_i^N|\}}{\mathbb{E}\{|\Omega_j^T|\}\pi R_N{}^2}$. Then, the average interference power from BSs in TN, equivalently denoted as $\Upsilon_T^{\text{Case 1}}(l)$, is expressed with closed-form as follows

$$\begin{aligned}
\Upsilon_T^{\text{Case 1}}(l) &= \mathbb{E}\left\{I_k^{T,\text{Case 1}}\right\} \\
&= \mathbb{E}\left\{\sum_{j'\in\Phi^T, j'\neq j}\left|\mathbf{g}_{j'k}^{\mathrm{H}}\mathbf{b}_{j'U(j')}\sqrt{P_{j'U(j')}^T}x_{U(j')}\right|^2\right\} \\
&= \mathbb{E}\left\{P_T\beta_0^T\sum_{j'\in\Phi^T, j'\neq j}\Lambda_{I,j'k'}^T l_{j'k}{}^{-\alpha_T}\right\} \\
&\overset{(a)}{=} \mathbb{E}\left\{P_T\beta_0^T\sum_{j'\in\Phi^T, j'\neq j} l_{j'k}{}^{-\alpha_T}\right\} \\
&= P_T\beta_0^T 2\pi\lambda_{TN}\int_l^\infty v^{-\alpha_T+1}dv \\
&\overset{(b)}{=} P_T\beta_0^T\pi\lambda_{TN}\frac{2}{\alpha_T-2}l^{2-\alpha_T}, \quad (55)
\end{aligned}$$

where (a) holds true because $\mathbb{E}\{\Lambda_{I,j'k'}^T\} = 1$, while (b) follows from the fact that $\int_l^\infty v^{-\alpha_T+1}dv = \frac{l^{2-\alpha_T}}{\alpha_T-2}$. Note that (53) and (55) are closed-form expressions which can be calculated directly. In addition, (53) and (55) are the functions of r and l whose PDFs are given in (21) and (27).

By inserting (38), (39), (40), as shown at the bottom of the previous page, (53), (55) into (41) and taking the definite integrals, we represent the coverage probability conditioned on Case 1 in (51) at the bottom of the page. Note that the expression of the coverage probability involves only two integrals which can be calculated efficiently.

$$\begin{aligned}
&\mathbb{P}\left\{\mathrm{SINR}_k^{\text{Case 1}} \geq \gamma_{th}\middle|\text{Case 1}\right\} \\
&\approx 1 - \int_{r_{I,\min}^N}^{r_{I,\max}^N}\int_{r_{DS,\min}^T}^{R_T} f_{r_{ik}}(r) f_{l_{jk}}(l)\left\{\frac{1}{\Gamma(\psi(r,l))}\gamma\left(\psi(r,l), \frac{\gamma_{th}\left(\Upsilon_N^{\text{Case 1}}(r) + \Upsilon_T^{\text{Case 1}}(l) + B_{1,3}\sigma_{n_0}{}^2\right)}{\zeta(r,l)}\right)\right\} dl dr. \quad (51)
\end{aligned}$$

B. CASE 2

In Case 2, we consider the coverage probability conditioned on that the typical user is only scheduled by a terrestrial BS in the current time slot. The are no desired signals from satellites so that the target signal for analysis is y_k^T in (12) and (11).

Regarding the desired signal from TN based on MRTBF, we have

$$\left|\mathbf{g}_{jk}^{\mathrm{H}}\mathbf{b}_{jk}\right|^2 = \left|\mathbf{g}_{jk}^{\mathrm{H}}\frac{\mathbf{g}_{jk}^{\mathrm{H}}}{\|\mathbf{g}_{jk}\|}\right|^2 = \beta_0^T {l_{jk}}^{-\alpha_T}\Lambda_{DS,j}^T, \tag{56}$$

where $\Lambda_{DS,j}^T \sim \Gamma(M_T, 1)$. Correspondingly, the desired signal power from TN in (34) can be rewritten as

$$\begin{aligned} DS_k^T &= \left|\sqrt{\beta_0^T {l_{jk}}^{-\alpha_T}\Lambda_{DS,j}^T}\sqrt{P_{jk}^T}x_k\right|^2 \\ &= \beta_0^T P_T {l_{jk}}^{-\alpha_T}\Lambda_{DS,j}^T. \end{aligned} \tag{57}$$

The CDF of $|\mathbf{g}_{jk}^{\mathrm{H}}\mathbf{b}_{jk}|^2$ is then given by

$$\begin{aligned} \mathbb{P}\left\{\left|\mathbf{g}_{jk}^{\mathrm{H}}\mathbf{b}_{jk}\right|^2 \le x\right\} &= \mathbb{P}\left\{\Lambda_{DS,j}^T \le \frac{x}{\beta_0^T {l_{jk}}^{-\alpha_T}}\right\} \\ &\approx \left(1-\exp\left(-B_h\frac{x}{\beta_0^T {l_{jk}}^{-\alpha_T}}\right)\right)^{M_T}, \end{aligned} \tag{58}$$

where $B_h = \Gamma(M_T+1)^{-\frac{1}{M_T\cdot\mathrm{scale}}}$. By inserting the interference power generated from TN, i.e., $I_k^{T,\mathrm{Case\ 2}}$, the coverage probability of the k-th user associated with the j-th BS is given by

$$\begin{aligned} &\mathbb{P}\left\{\mathrm{SINR}_k^{\mathrm{Case\ 2}} \ge \gamma_{th}\middle|\mathrm{Case\ 2}\right\} \\ &= \mathbb{P}\left\{\frac{DS_k^T}{I_k^{T,\mathrm{Case\ 2}} + B_2{\sigma_{n_0}}^2} \ge \gamma_{th}\right\} \\ &= \mathbb{P}\left\{\beta_0^T P_T {l_{jk}}^{-\alpha_T}\Lambda_{DS,j}^T \ge \gamma_{th}\left(I_k^{T,\mathrm{Case\ 2}} + B_2{\sigma_{n_0}}^2\right)\right\} \\ &= \mathbb{P}\left\{\Lambda_{DS,j}^T \ge \frac{\gamma_{th}}{\beta_0^T P_T {l_{jk}}^{-\alpha_T}}\left(I_k^{T,\mathrm{Case\ 2}} + B_2{\sigma_{n_0}}^2\right)\right\} \\ &\overset{(a)}{=} 1 - \mathbb{E}_{l_{jk}}\left\{\sum_{q=0}^{\infty}\binom{M_T}{q}(-1)^q\mathcal{L}_{I_k^{T,\mathrm{Case\ 2}}}(s)e^{-sB_2{\sigma_{n_0}}^2}\right\}, \end{aligned}$$

where (a) is obtained from $s = \frac{q\cdot B_h\gamma_{th}}{\beta_0^T P_T {l_{jk}}^{-\alpha_T}}$.

The density of interfering BSs in frequency band B_2 is $\lambda_{TT} = \lambda_T - \lambda_{TN}$. Then, the Laplace transform of interference power generated from TN is given by (59) at the bottom of the page, where (a) is achieved by $\hat{s} = sP_T\beta_0^T = qB_h\gamma_{th}{l_{jk}}^{\alpha_T}$, (b) follows from probability generating functional (PGFL) of the PPP [55], (c) is because the square root of the gamma distribution, $\sqrt{\Lambda_{I,j'k'}^T}$, follows the Nakagami distribution, (d) holds from $T_k^{T,\mathrm{Case\ 2}} = qB_h\gamma_{th}$. By taking $u = (v^{-1}l_{jk}(T_k^{T,\mathrm{case\ 2}})^{\frac{1}{\alpha_T}})^{-2}$, (59), also denoted as $\Upsilon_T^{\mathrm{Case\ 2}}(l)$, can be further expressed with closed-form as

$$\begin{aligned} &\mathcal{L}_{I_k^{T,\mathrm{case\ 2}}}(s) \\ &= \exp\left(-\pi\lambda_{TT}{l_{jk}}^2\left(T_k^{T,\mathrm{Case\ 2}}\right)^{\frac{2}{\alpha_T}}\right. \\ &\qquad\left.\times\int_{\left(T_k^{T,\mathrm{Case\ 2}}\right)^{-\frac{2}{\alpha_T}}}^{\infty}\left(\frac{1}{1+u^{\frac{\alpha_T}{2}}}\right)du\right) \\ &= \exp\left(-\pi\lambda_{TT}{l_{jk}}^2\frac{2}{\alpha_T-2}T_k^{T,\mathrm{Case\ 2}}\right. \\ &\qquad\left.\times\ {}_2F_1\left[1, 1-\frac{2}{\alpha_T}; 2-\frac{2}{\alpha_T}; -T_k^{T,\mathrm{Case\ 2}}\right]\right) \\ &= \Upsilon_T^{\mathrm{Case\ 2}}(l). \end{aligned}$$

$$\begin{aligned} \mathcal{L}_{I_k^{T,\mathrm{Case\ 2}}}(s) &= \mathbb{E}\left\{\exp\left(-sI_k^{T,\mathrm{Case\ 2}}\right)\right\} \\ &= \mathbb{E}\left\{\exp\left[-s\sum_{j'\in\Phi^{TT},j'\ne j}\left|\mathbf{g}_{j'k}^{\mathrm{H}}\mathbf{b}_{j'U(j')}\sqrt{P_{j'U(j')}^T}x_{U(j')}\right|^2\right]\right\} \\ &\overset{(a)}{=} \mathbb{E}\left\{\exp\left(-\hat{s}\sum_{j'\in\Phi^{TT},j'\ne j}\Lambda_{I,j'k'}^T {l_{j'k}}^{-\alpha_T}\right)\right\} \\ &= \mathbb{E}_{\Phi^{TT}}\left\{\prod_{j'\in\Phi^T,j'\ne j}\mathbb{E}_{\Lambda_{I,j'k'}^T}\left\{\exp\left(-\hat{s}\Lambda_{I,j'k'}^T {l_{j'k}}^{-\alpha_T}\right)\right\}\right\} \\ &\overset{(b)}{=} \exp\left(-2\pi\lambda_{TT}\int_{l_{jk}}^{\infty}\left(1-\mathbb{E}_{\Lambda_{I,j'k'}^T}\left[e^{-\hat{s}\Lambda_{I,j'k'}^T v^{-\alpha_T}}\right]\right)vdv\right) \\ &\overset{(c)}{=} \exp\left(-2\pi\lambda_{TT}\int_{l_{jk}}^{\infty}\left(1-\frac{1}{1+\hat{s}v^{-\alpha_T}}\right)vdv\right) \\ &\overset{(d)}{=} \exp\left(-2\pi\lambda_{TT}\int_{l_{jk}}^{\infty}\left(1-\frac{1}{1+T_k^{T,\mathrm{Case\ 2}}{l_{jk}}^{\alpha_T}v^{-\alpha_T}}\right)vdv\right), \end{aligned} \tag{59}$$

By inserting (63), as shown at the bottom of the next page to (59), we obtain the coverage probability conditioned on Case 2 in (60), as shown at the bottom of the page.

C. CASE 3

For Case 3, we derive the coverage probability of a typical user conditioned on the fact that it is only scheduled by a satellite in a time slot. Since there are no desired signals from terrestrial BSs, the target signal for analysis is y_k^N in (8) and (14).

Based on the ZFBF, the CDF of $|\mathbf{h}_{ik}^{\mathrm{H}}\mathbf{w}_k|^2$ is given by

$$\begin{aligned}&\mathbb{P}\left\{\left|\mathbf{h}_{ik}^{\mathrm{H}}\mathbf{w}_k\right|^2 \le x\right\}\\&= \mathbb{P}\left\{\Lambda_{DS,k}^N \le \frac{x}{\beta_0^N {r_{ik}}^{-\alpha_N}}\right\}\\&\approx \left(1-\exp\left(-A_h\frac{x}{\beta_0^N {r_{ik}}^{-\alpha_N}}\right)\right)^{(M_N-K+1)\kappa},\end{aligned} \tag{61}$$

where $A_h = \Gamma((M_N-K+1)\kappa+1)^{-\frac{1}{(M_N-K+1)\kappa\cdot\mathrm{scale}}}$, and the above equality holds when $M_N = K$.

By inserting $DS_k^N = |\mathbf{h}_{ik}^{\mathrm{H}}\mathbf{w}_k\sqrt{G_{ml}}\sqrt{P_k^N}x_k|^2$, the coverage probability of the k-th user associated with the i-th satellite for Case 3 is given by (62) at the bottom of the page, where (a) is obtained by the approximation of normalized gamma distribution of $|\mathbf{h}_{ik}^{\mathrm{H}}\mathbf{w}_k|^2$ [59], (b) is obtained from Binomial theorem, $s = \frac{q\cdot A_h\gamma_{th}}{G_{ml}P_k^N\beta\beta_0^N {r_{ik}}^{-\alpha_N}}$, and $P_k^N = \frac{P_N}{\mathbb{E}\{|\Omega_i^N|\}}$ is denoted for equal power allocation.

First, the Laplace transform of interference power I_k^N from NTN in Case 3, equivalently denoted as $\Upsilon_N^{\mathrm{Case\ 3}}(r)$, is given by (63) at the top of the next page, where (a) is obtained from $\hat{s} = s\cdot\frac{P_N}{\mathbb{E}\{|\Omega_i^N|\}}G_{sl}\beta\beta_0^N$, (b) holds true for the PGFL of the PPP, (c) is because $\sqrt{\Lambda_{I,i'k}^N}$ follows from the Nakagami-m distribution, and (d) is from denoting $T_k^N = q\frac{G_{sl}}{G_{ml}}A_h\gamma_{th}\mathbb{E}\{|\Omega_{i'}^N|\}$.

Let $u = (v^{-1}r_{ik}(T_k^N)^{\frac{1}{\alpha_N}})^{-2}$, we derive the Laplace transform of I_k^N in (64) at the bottom of the next page after next, where (a) follows from the fact that

$$\begin{aligned}&\left(r_{I,\max}^N\right)^2 {r_{ik}}^{-2}\left(T_k^N\right)^{-\frac{2}{\alpha_N}}\\&= \left[\left(r_{I,\max}^N\right)^{\alpha_N}{r_{ik}}^{-\alpha_N}\left(T_k^N\right)^{-1}\right]^{\frac{2}{\alpha_N}},\end{aligned} \tag{65}$$

and the integral is represented by a hypergeometric function as follows

$$\int_{T^{\frac{2}{\alpha}}}^{\infty}\frac{1}{1+u^{\frac{\alpha}{2}}}du = \frac{2T^{\frac{2}{\alpha_N}-1}}{\alpha-2}{}_2F_1\left[1,1-\frac{2}{\alpha};2-\frac{2}{\alpha};-\frac{1}{T}\right]. \tag{66}$$

Second, the Laplace transform of interference power from TN in Case 3, i.e., of $I_k^{T,\mathrm{Case\ 3}}$, is given by

$$\begin{aligned}\mathcal{L}_{I_k^{T,\mathrm{Case\ 3}}}(s) &= \mathbb{E}\left\{\exp\left(-sI_k^{T,\mathrm{Case\ 3}}\right)\right\}\\&= \mathbb{E}\left\{\exp\left[-s\sum_{j'\in\Phi^T}\left|\mathbf{g}_{j'k}^{\mathrm{H}}\mathbf{b}_{j'U(j')}\sqrt{P_{j'U(j')}^T}x_{U(j')}\right|^2\right]\right\}\\&= \exp\left(-2\pi\lambda_T\int_{r_{I,\min}^T}^{\infty}\left(1-\frac{1}{1+sP_T\beta_0^T v^{-\alpha_T}}\right)vdv\right)\\&= \exp\left(-\pi\lambda_T {r_{ik}}^{\alpha_N} {r_{I,\min}^T}^{2-\alpha_T}\frac{2}{\alpha_T-2}T_k^{T,\mathrm{Case\ 3}}\right.\\&\quad\left.\times\ {}_2F_1\left[1,1-\frac{2}{\alpha_T};2-\frac{2}{\alpha_T};-{r_{ik}}^{\alpha_N}{r_{I,\min}^T}^{-\alpha_T}T_k^{T,\mathrm{Case\ 3}}\right]\right).\end{aligned} \tag{67}$$

$$\mathbb{P}\left\{\mathrm{SINR}_k^{\mathrm{Case\ 2}} \ge \gamma_{th}\middle|\mathrm{Case\ 2}\right\} = 1-\int_{r_{DS,\min}^T}^{R_T} f_{l_{jk}}(l)\left[\sum_{q=0}^{\infty}\binom{M_T}{q}(-1)^q\Upsilon_T^{\mathrm{Case\ 2}}(l)e^{-\frac{q\cdot B_h\gamma_{th}}{\beta_0^T P_T l^{-\alpha_T}}{B_2\sigma_{n_0}}^2}\right]dl, \tag{60}$$

$$\begin{aligned}\mathbb{P}\left\{\mathrm{SINR}_k^{\mathrm{Case\ 3}} \ge \gamma_{th}\middle|\mathrm{Case\ 3}\right\} &= \mathbb{P}\left\{\frac{\left|\mathbf{h}_{ik}^{\mathrm{H}}\mathbf{w}_k\sqrt{G_{ml}}\sqrt{P_k^N}x_k\right|^2}{I_k^N+I_k^{T,\mathrm{Case\ 3}}+{B_{1,3}\sigma_{n_0}}^2} \ge \gamma_{th}\right\}\\&= \mathbb{P}\left\{\left|\mathbf{h}_{ik}^{\mathrm{H}}\mathbf{w}_k\right|^2 \ge \frac{\gamma_{th}}{G_{ml}P_k^N}\left(I_k^N+I_k^{T,\mathrm{Case\ 3}}+{B_{1,3}\sigma_{n_0}}^2\right)\right\}\\&\overset{(a)}{\approx} 1-\mathbb{E}\left\{\left[1-\exp\left(-A_h\frac{\gamma_{th}\left(I_k^N+I_k^{T,\mathrm{Case\ 3}}+{B_{1,3}\sigma_{n_0}}^2\right)}{G_{ml}P_k^N\beta\beta_0^N {r_{ik}}^{-\alpha_N}}\right)\right]^{(M_N-K+1)\kappa}\right\}\\&\overset{(b)}{=} 1-\sum_{q=0}^{\infty}\binom{(M_N-K+1)\kappa}{q}\times\mathbb{E}\left\{-e^{-A_h\frac{\gamma_{th}\left(I_k^N+I_k^{T,\mathrm{Case\ 3}}+{B_{1,3}\sigma_{n_0}}^2\right)}{G_{ml}P_k^N\beta\beta_0^N {r_{A(k)k}}^{-\alpha_N}}}\right\}^q\\&\approx 1-\sum_{q=0}^{\infty}\binom{(M_N-K+1)\kappa}{q}\times(-1)^q\mathcal{L}_{I_k^N}(s)\mathcal{L}_{I_k^{T,\mathrm{Case\ 3}}}(s)e^{-s{B_{1,3}\sigma_{n_0}}^2},\end{aligned} \tag{62}$$

Finally, after inserting (64) and (67) into (62), the coverage probability conditioned on Case 3 is represented as (68) at the bottom of the next page.

V. SIMULATION RESULTS AND DISCUSSION

In this section, we quantitatively evaluate the downlink performance of the multi-connectivity MIMO between TN

$$
\begin{aligned}
\mathcal{L}_{I_k^N}(s) &= \Upsilon_N^{\text{Case 3}}(r) \\
&= \mathbb{E}\left\{\exp\left(-sI_k^N\right)\right\} \\
&= \mathbb{E}\left\{\exp\left(-s\sum_{k'\notin\Omega_i^N}\left|\mathbf{h}_{A(k')k}^{\mathrm{H}}\mathbf{w}_{k'}\sqrt{G_{sl}}\sqrt{P_{k'}^N}x_{k'}\right|^2\right)\right\} \\
&= \mathbb{E}\left\{\exp\left(-s\sum_{i'\in\Phi^N,i'\neq i}\sum_{k'\in\Omega_{i'}^N}\left|\mathbf{h}_{i'k}^{\mathrm{H}}\mathbf{w}_{k'}\sqrt{G_{sl}}\sqrt{P_{k'}^N}x_{k'}\right|^2\right)\right\} \\
&\overset{(a)}{=} \mathbb{E}\left\{\exp\left(-\hat{s}\sum_{i'\in\Phi^N,i'\neq i}\sum_{k'\in\Omega_{i'}^N}\Lambda_{I,i'k}^N {r_{i'k}}^{-\alpha_N}\right)\right\} \\
&= \mathbb{E}_{\Phi^N}\left\{\prod_{i'\in\Phi^N,i'\neq i}\mathbb{E}_{\Omega_{i'}^N}\left\{\prod_{k'\in\Omega_{i'}^N}\exp\left(-\hat{s}\Lambda_{I,i'k}^N {r_{i'k}}^{-\alpha_N}\right)\right\}\right\} \\
&\overset{(b)}{=} \exp\left(-2\pi\lambda_N\frac{R_S}{R_E}\int_{r_{ik}}^{r_{I,\max}^N}\left(1-\mathbb{E}\left[e^{-\hat{s}\mathbb{E}\left\{\left|\Omega_{i'}^N\right|\right\}\Lambda_{I,i'k}^N v^{-\alpha_N}}\right]\right)vdv\right) \\
&\overset{(c)}{=} \exp\left(-2\pi\lambda_N\frac{R_S}{R_E}\int_{r_{ik}}^{r_{I,\max}^N}\left(1-\frac{1}{1+\hat{s}\mathbb{E}\left\{\left|\Omega_{i'}^N\right|\right\}v^{-\alpha_N}}\right)vdv\right) \\
&\overset{(d)}{=} \exp\left(-2\pi\lambda_N\frac{R_S}{R_E}\int_{r_{ik}}^{r_{I,\max}^N}\left(1-\frac{1}{1+T_k^N {r_{ik}}^{\alpha_N}v^{-\alpha_N}}\right)vdv\right) \\
&= \exp\left(-2\pi\lambda_N\frac{R_S}{R_E}\int_{r_{ik}}^{r_{I,\max}^N}\left(\frac{T_k^N}{T_k^N+\left(\frac{v}{r_{ik}}\right)^{\alpha_N}}\right)vdv\right),
\end{aligned}
\tag{63}
$$

$$
\begin{aligned}
\mathcal{L}_{I_k^N}(s) &= \exp\left(-\pi\lambda_N\frac{R_S}{R_E}{r_{ik}}^2\left(T_k^N\right)^{\frac{2}{\alpha_N}}\int_{\left(T_k^N\right)^{-\frac{2}{\alpha_N}}}^{\left(\frac{r_{I,\max}^N}{r_{ik}\left(T_k^N\right)^{\frac{1}{\alpha_N}}}\right)^2}\left(\frac{1}{1+u^{\frac{\alpha_N}{2}}}\right)du\right) \\
&= \exp\left(-\pi\lambda_N\frac{R_S}{R_E}{r_{ik}}^2\left(T_k^N\right)^{\frac{2}{\alpha_N}}\left[\int_{\left(T_k^N\right)^{-\frac{2}{\alpha_N}}}^{\infty}\left(\frac{1}{1+u^{\frac{\alpha_N}{2}}}\right)du-\int_{\left(r_{I,\max}^N\right)^2 {r_{ik}}^{-2}\left(T_k^N\right)^{-\frac{2}{\alpha_N}}}^{\infty}\left(\frac{1}{1+u^{\frac{\alpha_N}{2}}}\right)du\right]\right) \\
&\overset{(a)}{=} \exp\left(-\pi\lambda_N\frac{R_S}{R_E}{r_{ik}}^2\left(T_k^N\right)^{\frac{2}{\alpha_N}}\frac{2}{\alpha_N-2}\left[\left(T_k^N\right)^{1-\frac{2}{\alpha_N}}{}_2F_1\left[1,1-\frac{2}{\alpha_N};2-\frac{2}{\alpha_N};-T_k^N\right]\right.\right. \\
&\qquad\left.\left.-\left(\frac{r_{ik}}{r_{I,\max}^N}\right)^{\alpha_N-2}\left(T_k^N\right)^{1-\frac{2}{\alpha_N}}{}_2F_1\left[1,1-\frac{2}{\alpha_N};2-\frac{2}{\alpha_N};-\left(\frac{r_{ik}}{r_{I,\max}^N}\right)^{\alpha_N}T_k^N\right]\right]\right) \\
&= \exp\left(-\pi\lambda_N\frac{R_S}{R_E}{r_{ik}}^2T_k^N\frac{2}{\alpha_N-2}\left[{}_2F_1\left[1,1-\frac{2}{\alpha_N};2-\frac{2}{\alpha_N};-T_k^N\right]\right.\right. \\
&\qquad\left.\left.-\left(\frac{r_{ik}}{r_{I,\max}^N}\right)^{\alpha_N-2}{}_2F_1\left[1,1-\frac{2}{\alpha_N};2-\frac{2}{\alpha_N};-\left(\frac{r_{ik}}{r_{I,\max}^N}\right)^{\alpha_N}T_k^N\right]\right]\right).
\end{aligned}
\tag{64}
$$

TABLE 1. Simulation parameters.

Parameter	Value
Radius of Earth	6,371.393 km
BS transmit power	40 W
Satellite density	5×10^{-13} / m^2
Satellite transmit power	100 W
Satellite antenna gain of main lobe	1,000
Satellite antenna gain of side lobe	10
Noise power	10^{-14} W
TN bandwidth	100 MHz

and NTN from a system-level perspective. On the one hand, the coverage probabilities are compared among different satellite altitudes and NTN path-loss exponents. On the other hand, the average achievable data rate of the typical user is investigated in terms of different satellite antenna numbers, TN path-loss exponents, ground BS density, and satellite bandwidth. The numerical results are provided according to related mathematical tools and expressions in Sections II–IV.

For the simulation and numerical results, we utilize MATLAB in Monte Carlo simulation manner to obtain the coverage probability and the average achievable data rate of a typical user in the satellite-terrestrial multi-connectivity MIMO system. In all iterations, main systematic parameters are summarized in Table 1 unless otherwise noted according to [60], while other parameters are determined based on specific scenarios. Particularly, the approximation of $\alpha_N \approx 2.0$ is for $\alpha_N = 2 + 1e^{-10}$. The density of BSs, i.e., λ_T, is 6×10^{-9} / m^2 and the average number of users associated with each BS, i.e., U_T, is 4. For comparison, TN scenario settings from [36], [37] are simulated as the baseline results of TN single-connectivity.

The coverage probability of the multi-connectivity system is plotted and compared against the SINR threshold under different satellite altitudes in Fig. 3. The corresponding closed-form expression is achieved by inserting expressions of connection probability (29), (30), (31), and expressions of coverage probability for each case (51), (60), (62) into (17). It is shown that when the satellite altitude decreases from 900 km to 300 km, the coverage probability increases under a given SINR threshold between −20 dB and 40 dB. This implies that in the introduced multi-connectivity model, higher satellite altitude incurs lower coverage probability at a specific SINR threshold range. It is also manifest from this figure that the analytical expression of the coverage probability perfectly matches with the simulation results.

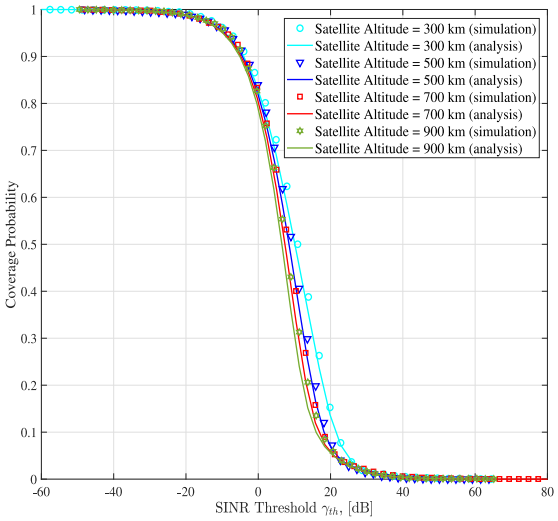

FIGURE 3. Coverage probability of the multi-connectivity system versus SINR threshold under different satellite altitudes, where $\alpha_N \approx 2.0$, $\alpha_T = 3.5$, $B_{1,3} = 200$ MHz, each satellite equipped with 4 antennas.

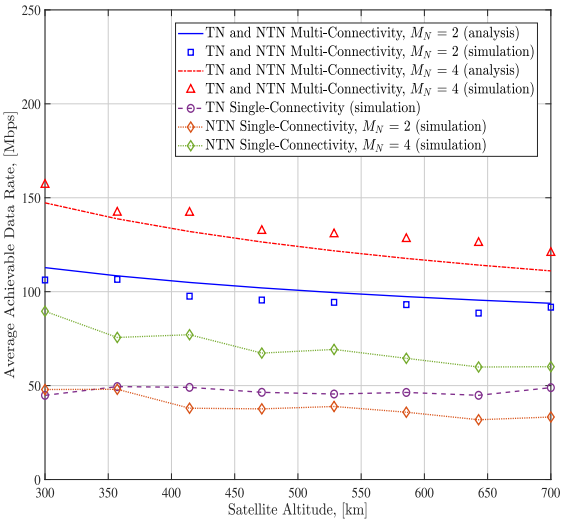

FIGURE 4. Average achievable data rate of the typical user versus satellite altitude under different satellite antenna numbers and connectivity statuses, where $\alpha_N \approx 2.0$, $\alpha_T = 3.5$, $B_{1,3} = 200$ MHz.

Fig. 4 compares the average achievable data rate of multi-connectivity systems under different satellite antenna numbers with TN single-connectivity and NTN single-connectivity, respectively. The closed-form expression for this data rate is obtained by inserting expressions of connection probability (29), (30), (31), as well as expressions of coverage probability for each case (51), (60), (62),

$$\mathbb{P}\left\{ \mathrm{SINR}_k^{\text{Case 3}} \geq \gamma_{th} \middle| \text{Case 3} \right\}$$
$$\approx 1 - \int_{r_{I,\min}^N}^{r_{I,\max}^N} f_{r_{ik}}(r) \sum_{q=0}^{\infty} \binom{(M_N - K + 1)\kappa}{q} (-1)^q \Upsilon_N^{\text{Case 3}}(r) \Upsilon_T^{\text{Case 3}}(r) e^{-\frac{q \cdot A_h \gamma_{th} \mathbb{E}\left\{ \left| \Omega_i^N \right| \right\}}{G_{ml} P_N \beta \beta_0^N r^{-\alpha_N}} B_{1,3} {\sigma_{n_0}}^2} dr. \quad (68)$$

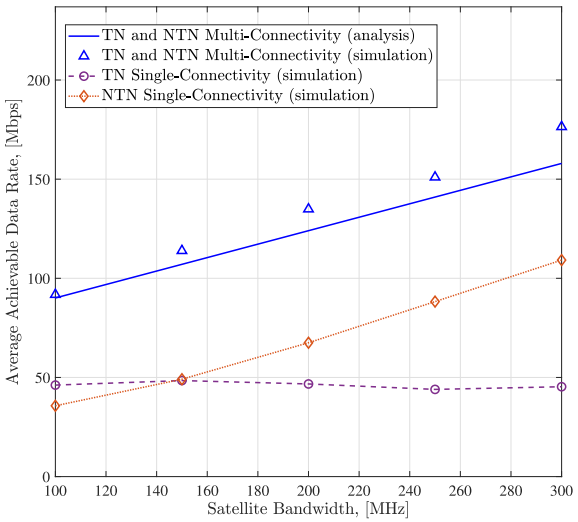

FIGURE 5. Average achievable data rate of the typical user versus satellite bandwidth, where $\alpha_N \approx 2.0$, $\alpha_T = 3.5$, each satellite equipped with 4 antennas while at an altitude of 500 km.

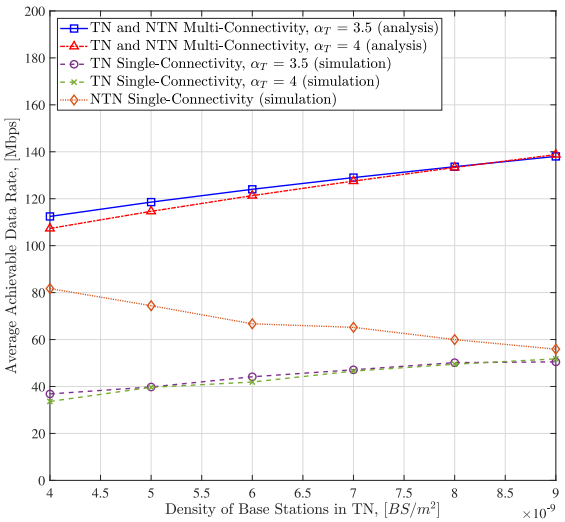

FIGURE 6. Average achievable data rate of the typical user versus density of BSs in TN, where $\alpha_N \approx 2.0$, $B_{1,3} = 200$ MHz, each satellite equipped with 4 antennas while at an altitude of 500 km.

into (20) and integral over variable t. As the satellite altitude increases, the general trend of the average achievable data rate in satellite-assisted systems decreases. This is because a higher altitude brings a more severe path-loss in the desired signal, which impairs the quality of service of the typical user associated with a satellite. Moreover, when increasing the number of satellite antennas from 2 to 4, the performance of average achievable data date can have at least 20% improvement. Also, the lower altitude brings smaller attenuation in the desired signal, and as a result of which the higher data rate increase can be achieved. The lower altitude is, the higher increase in data rate will be, which is owing to smaller attenuation in the desired signal. In the TN single-connectivity system, however, the average data rate remains virtually unchanged. This undoubtedly goes well with our intuition - the signals from ground BS are not related to the satellite altitude. Generally, the TN and NTN multi-connectivity systems significantly outperform the TN single-connectivity system or the NTN single-connectivity system. The results further illustrate the importance of investigating satellite-terrestrial integrated networks.

Fig. 5 illustrates the gap of average achievable data rate between the multi-connectivity scenario and the single-connectivity one with the increase of satellite bandwidth. The closed-form analytical expression for the average achievable data rate is obtained from (20). The average data rate for the TN single-connectivity shows almost no change, remaining constant at around 48 Mbps, since it is irrelevant to satellite bandwidth. On the contrary, the data rate for the NTN single-connectivity increases from 40 Mbps to 110 Mbps, while comparatively an approximate 40 Mbps increment can be seen for NTN multi-connectivity at each satellite bandwidth. It is thus concluded that with enough satellite bandwidth, the data rate provided by multi-connectivity between TN and NTN outperforms that by single-connectivity. Moreover, the Monte Carlo simulation results match well with the derived analytical results.

Finally, the influences of TN path-loss exponent α_T on both the multi-connectivity and the single-connectivity scenarios, under different densities of ground BSs, are demonstrated in Fig. 6. The closed-form analytical expression for the average achievable data rate is obtained from (20). As the BS density increases, the data rate for TN single-connectivity with $\alpha_T = 3.5$ is about 5 Mbps higher than that with $\alpha_T = 4$ under given BS density, while this gap narrows as the BS density increases. Another similar gap and trend are also witnessed for the two TN-NTN multi-connectivity counterparts. These two gaps arise from the fact that the increase in TN path-loss downgrades the quality of the desired signals from TN, and the interference due to the increasing BS density will have more impacts on the overall TN interference than that due to the TN path-loss, thus the gap in between is reduced. On the contrary, the only decreasing trend is witnessed for NTN single-connectivity. This is because while the desired signals of satellite communications remain constant, a higher density of ground BSs brings higher TN interference signals. Consequently, the performance of the overall average achievable data rate could be severely degraded.

VI. CONCLUSION

In this paper, we introduced and analyzed a multi-connectivity MIMO system between TN and NTN in terms of coverage performance and average achievable data rate. Using stochastic geometry and the Welch-Satterthwaite approximation, we modeled four different connection cases for the typical user. We derived approximated but tractable and closed-form expressions for the overall coverage

probability. The influences of critical system parameters, including satellite altitude, satellite antenna number, satellite bandwidth, the density of ground BSs, and path-loss exponents of TN and NTN, were involved in comparing the system performance between single-connectivity and multi-connectivity systems. In the introduced multi-connectivity MIMO system between TN and NTN, deployment of LEO satellites at lower altitudes will improve coverage probability and achievable data rate. Concerning the influences of path-loss exponents, we found that higher TN path-loss negatively affects the overall performance, while a slightly higher NTN path-loss contributes positively. Moreover, sufficient satellite antennas and bandwidth allocation are vital system parameters to ensure the high performance of the multi-connectivity TN and NTN systems.

REFERENCES

[1] T. Sylla, L. Mendiboure, S. Maaloul, H. Aniss, M. A. Chalouf, and S. Delbruel, "Multi-connectivity for 5G networks and beyond: A survey," *Sensors*, vol. 22, no. 19, p. 7591, 2022.

[2] M. Y. Abdelsadek, G. Karabulut-Kurt, H. Yanikomeroglu, P. Hu, G. Lamontagne, and K. Ahmed, "Broadband connectivity for handheld devices via leo satellites: Is distributed massive MIMO the answer?" *IEEE Open J. Commun. Soc.*, vol. 4, pp. 713–726, 2023.

[3] F. Rinaldi et al., "Non-terrestrial networks in 5G & beyond: A survey," *IEEE Access*, vol. 8, pp. 165178–165200, 2020.

[4] "Study on new radio (NR) to support non-terrestrial networks; (Release 15), Version 15.4.0," 3GPP, Sophia Antipolis, France, Rep. TR 38.811, Sep. 2020.

[5] "Solutions for NR to support non-terrestrial networks (NTN); (Release 16), Version 16.1.0," 3GPP, Sophia Antipolis, France, Rep. TR 38.821, May 2021.

[6] "Study on narrow-band Internet of Things (NB-IoT)/enhanced machine type communication (eMTC) support for non-terrestrial networks (NTN); (Release 17), Version 17.0.0," 3GPP, Sophia Antipolis, France, Rep. TR 36.763, Jun. 2021.

[7] "Solutions for NR to support non-terrestrial networks (NTN): Non-terrestrial networks (NTN) related RF and co-existence aspects; (Release 17), Version 17.0.0," 3GPP, Sophia Antipolis, France, Rep. TR 38.863, Jun. 2022.

[8] I. Leyva-Mayorga et al., "LEO small-satellite constellations for 5G and beyond-5G communications," *IEEE Access*, vol. 8, pp. 184955–184964, 2020.

[9] I. Del Portillo, B. G. Cameron, and E. F. Crawley, "A technical comparison of three low earth orbit satellite constellation systems to provide global broadband," *Acta Astronautica*, vol. 159, pp. 123–135, Jun. 2019.

[10] Y. Su, Y. Liu, Y. Zhou, J. Yuan, H. Cao, and J. Shi, "Broadband leo satellite communications: Architectures and key technologies," *IEEE Wireless Commun.*, vol. 26, no. 2, pp. 55–61, Apr. 2019.

[11] F. Vatalaro, G. E. Corazza, C. Caini, and C. Ferrarelli, "Analysis of LEO, MEO, and GEO global mobile satellite systems in the presence of interference and fading," *IEEE J. Sel. Areas Commun.*, vol. 13, no. 2, pp. 291–300, Feb. 1995.

[12] B. Shang, X. Li, C. Li, and Z. Li, "Coverage in cooperative leo satellite networks," *J. Commun. Inf. Netw.*, vol. 8, no. 4, pp. 329–340, Dec. 2023.

[13] J. N. Pelton and R. Laufer, "Commercial small satellites for business constellations including microsatellites and minisatellites," in *Handbook of Small Satellites: Technology, Design, Manufacture, Applications, Economics and Regulation*. Cham, Switzerland: Springer, 2019, pp. 1–20.

[14] A. J. Paulraj, D. A. Gore, R. U. Nabar, and H. Bolcskei, "An overview of MIMO communications-a key to gigabit wireless," *Proc. IEEE*, vol. 92, no. 2, pp. 198–218, Feb. 2004.

[15] T. L. Marzetta, "Massive MIMO: An introduction," *Bell Labs Techn. J.*, vol. 20, pp. 11–22, Mar. 2015. [Online]. Available: https://ieeexplore.ieee.org/abstract/document/7064850

[16] L. Lu, G. Y. Li, A. L. Swindlehurst, A. Ashikhmin, and R. Zhang, "An overview of massive MIMO: Benefits and challenges," *IEEE J. Sel. Topics Signal Process.*, vol. 8, no. 5, pp. 742–758, Oct. 2014.

[17] S. N. Chiu, D. Stoyan, W. S. Kendall, and J. Mecke, *Stochastic Geometry and its Applications*. Hoboken, NJ, USA: Wiley, 2013.

[18] C. K. Armeniakos, P. S. Bithas, and A. G. Kanatas, "Sir analysis in 3D UAV networks: A stochastic geometry approach," *IEEE Access*, vol. 8, pp. 204963–204973, 2020.

[19] H. ElSawy, E. Hossain, and M. Haenggi, "Stochastic geometry for modeling, analysis, and design of multi-tier and cognitive cellular wireless networks: A survey," *IEEE Commun. Surveys Tuts.*, vol. 15, no. 3, pp. 996–1019, 3rd Quart., 2013.

[20] X. Gu, B. Leng, L. Zhang, J. Miao, and L. Zhang, "A stochastic geometry approach to model and analyze future vehicular communication networks," *IEEE Access*, vol. 8, pp. 14500–14512, 2020.

[21] V. Petrov et al., "Dynamic multi-connectivity performance in ultra-dense urban mmWave deployments," *IEEE J. Sel. Areas Commun.*, vol. 35, no. 9, pp. 2038–2055, Sep. 2017.

[22] M. Giordani, M. Mezzavilla, S. Rangan, and M. Zorzi, "An efficient uplink multi-connectivity scheme for 5G millimeter-wave control plane applications," *IEEE Trans. Wireless Commun.*, vol. 17, no. 10, pp. 6806–6821, Oct. 2018.

[23] M.-T. Suer, C. Thein, H. Tchouankem, and L. Wolf, "Multi-connectivity as an enabler for reliable low latency communications—An overview," *IEEE Commun. Surveys Tuts.*, vol. 22, no. 1, pp. 156–169, 1st Quart., 2019.

[24] N. H. Mahmood and H. Alves, "Dynamic multi-connectivity activation for ultra-reliable and low-latency communication," in *Proc. 16th Int. Symp. Wireless Commun. Syst. (ISWCS)*, 2019, pp. 112–116.

[25] C. She, Z. Chen, C. Yang, T. Q. Quek, Y. Li, and B. Vucetic, "Improving network availability of ultra-reliable and low-latency communications with multi-connectivity," *IEEE Trans. Commun.*, vol. 66, no. 11, pp. 5482–5496, Nov. 2018.

[26] M.-T. Suer, C. Thein, H. Tchouankem, and L. Wolf, "Reliability and latency performance of multi-connectivity scheduling schemes in multi-user scenarios," in *Proc. 32nd Int. Teletraffic Congr. (ITC 32)*, 2020, pp. 73–80.

[27] A. Ravanshid et al., "Multi-connectivity functional architectures in 5G," in *Proc. IEEE Int. Conf. Commun. Workshops (ICC)*, 2016, pp. 187–192.

[28] X. Ba, "Qos-forecasting-based intelligent flow-control scheme for multi-connectivity in 5G heterogeneous networks," *IEEE Access*, vol. 9, pp. 104304–104315, 2021.

[29] D. S. Michalopoulos, I. Viering, and L. Du, "User-plane multi-connectivity aspects in 5G," in *Proc. 23rd Int. Conf. Telecommun. (ICT)*, 2016, pp. 1–5.

[30] M. Majamaa, "Toward multi-connectivity in beyond 5G non-terrestrial networks: Challenges and solutions," 2024, *arXiv:2310.10213*.

[31] M. Majamaa, H. Martikainen, L. Sormunen, and J. Puttonen, "Multi-connectivity for user throughput enhancement in 5G non-terrestrial networks," in *Proc. 18th Int. Conf. Wireless Mobile Comput., Netw. Commun. (WiMob)*, 2022, pp. 412–418.

[32] L. You, K.-X. Li, J. Wang, X. Gao, X.-G. Xia, and B. Ottersten, "Massive MIMO transmission for LEO satellite communications," *IEEE J. Sel. Areas Commun.*, vol. 38, no. 8, pp. 1851–1865, Aug. 2020.

[33] K.-X. Li et al., "Downlink transmit design for massive MIMO LEO satellite communications," *IEEE Trans. Commun.*, vol. 70, no. 2, pp. 1014–1028, Feb. 2022.

[34] M. Y. Abdelsadek, G. K. Kurt, and H. Yanikomeroglu, "Distributed massive MIMO for LEO satellite networks," *IEEE Open J. Commun. Soc.*, vol. 3, pp. 2162–2177, 2022.

[35] B. Hu et al., "LEO satellite vs. cellular networks: Exploring the potential for synergistic integration," in *Proc. Compan. 19th Int. Conf. Emerg. Netw. Exp. Technol.*, 2023, pp. 45–51.

[36] M. López, S. B. Damsgaard, I. Rodríguez, and P. Mogensen, "Connecting rural areas: An empirical assessment of 5G terrestrial-leo satellite multi-connectivity," in *Proc. IEEE 97th Veh. Technol. Conf. (VTC)*, 2023, pp. 1–5.

[37] M. López, S. B. Damsgaard, I. Rodríguez, and P. Mogensen, "An empirical analysis of multi-connectivity between 5G terrestrial and leo satellite networks," in *Proc. IEEE Globecom Workshops (GC Wkshps)*, 2022, pp. 1115–1120.

[38] M. Majamaa, H. Martikainen, J. Puttonen, and T. Hämäläinen, "Satellite-assisted multi-connectivity in beyond 5G," 2023, *arXiv:2304.12097*.
[39] T. Van Chien, H. A. Le, T. H. Tung, H. Q. Ngo, and S. Chatzinotas, "Joint power allocation and user scheduling in integrated satellite-terrestrial cell-free massive MIMO IoT systems," 2024, *arXiv:2401.03754*.
[40] A. Talgat, M. A. Kishk, and M.-S. Alouini, "Stochastic geometry-based analysis of leo satellite communication systems," *IEEE Commun. Lett.*, vol. 25, no. 8, pp. 2458–2462, Aug. 2021.
[41] R. Deng, B. Di, H. Zhang, L. Kuang, and L. Song, "Ultra-dense leo satellite constellations: How many leo satellites do we need?" *IEEE Trans. wireless Commun.*, vol. 20, no. 8, pp. 4843–4857, Aug. 2021.
[42] N. Cassiau et al., "Satellite and terrestrial multi-connectivity for 5G: Making spectrum sharing possible," in *Proc. IEEE Wireless Commun. Netw. Conf. Workshops (WCNCW)*, 2020, pp. 1–6.
[43] H. Chung, J. Kim, G. Noh, S. H. Won, T. Choi, and I. Kim, "Demonstration of service continuity based on multi-connectivity with cellular and satellite access networks," in *Proc. Int. Conf. Inf. Commun. Technol. Converg. (ICTC)*, 2021, pp. 1400–1402.
[44] N. Cassiau et al., "5G-ALLSTAR: Beyond 5G satellite-terrestrial multi-connectivity," in *Proc. Joint Eur. Conf. Netw. Commun. 6G Summit (EuCNC/6G Summit)*, 2022, pp. 148–153.
[45] P. Yue, J. Du, R. Zhang, H. Ding, S. Wang, and J. An, "Collaborative LEO satellites for secure and green Internet of Remote Things," *IEEE Internet Things J.*, vol. 10, no. 11, pp. 9283–9294, Jun. 2023.
[46] S. Kota and G. Giambene, "Satellite 5G: IoT use case for rural areas applications," in *Proc. 11th Int. Conf. Adv. Satell. Space Commun. (SPACOMM)*, 2019, pp. 24–28.
[47] A. Abdi, W. C. Lau, M.-S. Alouini, and M. Kaveh, "A new simple model for land mobile satellite channels: First-and second-order statistics," *IEEE Trans. Wireless Commun.*, vol. 2, no. 3, pp. 519–528, May 2003.
[48] H. Jia, Z. Ni, C. Jiang, L. Kuang, and J. Lu, "Uplink interference and performance analysis for megasatellite constellation," *IEEE Internet Things J.*, vol. 9, no. 6, pp. 4318–4329, Mar. 2022.
[49] H. Jia, C. Jiang, L. Kuang, and J. Lu, "An analytic approach for modeling uplink performance of mega constellations," *IEEE Trans. Veh. Technol.*, vol. 72, no. 2, pp. 2258–2268, Feb. 2023.
[50] G. Zheng, S. Chatzinotas, and B. Ottersten, "Generic optimization of linear precoding in multibeam satellite systems," *IEEE Trans. Wireless Commun.*, vol. 11, no. 6, pp. 2308–2320, Jun. 2012.
[51] D. Christopoulos, S. Chatzinotas, and B. Ottersten, "Multicast multigroup precoding and user scheduling for frame-based satellite communications," *IEEE Trans. Wireless Commun.*, vol. 14, no. 9, pp. 4695–4707, Sep. 2015.
[52] V. Joroughi, M. Á. Vázquez, and A. I. Pérez-Neira, "Precoding in multigateway multibeam satellite systems," *IEEE Trans. Wireless Commun.*, vol. 15, no. 7, pp. 4944–4956, Jul. 2016.
[53] R. T. Schwarz, T. Delamotte, K.-U. Storek, and A. Knopp, "MIMO applications for multibeam satellites," *IEEE Trans. Broadcast.*, vol. 65, no. 4, pp. 664–681, Dec. 2019.
[54] B. V. Gnedenko, *Theory of Probability*. Boca Raton, FL, USA: Routledge, 2018.
[55] M. Haenggi, *Stochastic Geometry for Wireless Networks*. Cambridge, U.K.: Cambridge Univ. Press, 2012.
[56] P. G. Moschopoulos, "The distribution of the sum of independent gamma random variables," *Annals Inst. Stat. Math.*, vol. 37, no. 1, pp. 541–544, 1985.
[57] C. Zhu and W. Yu, "Stochastic modeling and analysis of user-centric network MIMO systems," *IEEE Trans. Commun.*, vol. 66, no. 12, pp. 6176–6189, Dec. 2018.
[58] E. Adebola and A. Annamalai, "Further results on the asymptotic analysis of digital communications in generalized fading channels," in *Proc. IEEE Asia Pac. Conf. Wireless Mobile*, 2014, pp. 23–29.
[59] B. Shang, L. Liu, R. M. Rao, V. Marojevic, and J. H. Reed, "3D spectrum sharing for hybrid D2D and UAV networks," *IEEE Trans. Commun.*, vol. 68, no. 9, pp. 5375–5389, Sep. 2020.
[60] S. Liu et al., "Leo satellite constellations for 5G and beyond: How will they reshape vertical domains?" *IEEE Commun. Mag.*, vol. 59, no. 7, pp. 30–36, Jul. 2021.

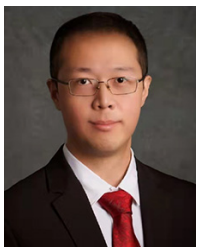

BODONG SHANG (Member, IEEE) received the B.Eng. degree from the School of Information Science and Technology, Northwest University, Xi'an, China, in 2015, the M.S. degree from the School of Telecommunications Engineering, Xidian University, Xi'an, in 2018, and the Ph.D. degree from the Department of Electrical and Computer Engineering, Virginia Tech, Blacksburg, USA, in 2021. He was a Postdoctoral Research Associate with Carnegie Mellon University, Pittsburgh, USA. He is currently an Assistant Professor with the Eastern Institute for Advanced Study, Eastern Institute of Technology, Ningbo, China. His current research areas are wireless communications and networking, including nonterrestrial networks, space–air–ground–sea integrated networks, vehicular communications, and edge computing. He received the Chinese Government Award for outstanding self-financed students abroad in 2021, the "6G Rising Star" Young Scholar in Global 6G Conference 2024, and held a summer research internship position at Nokia Bell Labs, USA, in 2021.

XIANGYU LI received the B.Eng. degree in electronic information engineering from Nantong University, Nantong, China, in June 2021, and the M.S. degree in electrical and computer engineering from the Georgia Institute of Technology, Atlanta, USA, in May 2023. He is currently pursuing the Ph.D. degree with Shanghai Jiao Tong University, Shanghai, China, in the EIT-SJTU Joint Ph.D. Program. His research interests include space–air–ground integrated networks, massive MIMO, integrated sensing and communication, physical-layer security, and performance analysis of wireless systems.

ZHUHANG LI received the B.S. degree from the University of Electronic Science and Technology of China, Chengdu, China, in 2022, and the M.S. degree from Nanyang Technological University in 2023. She is a Research Assistant with the Eastern Institute for Advanced Study, Eastern Institute of Technology, Ningbo, China. Her research interests include space–air–ground–sea integrated networks and Internet of Things.

JUNCHAO MA (Member, IEEE) received the Ph.D. degree from the Department of Information Science and Technology, Southwest Jiaotong University in 2020. From 2017 to 2019, he was a Visiting Scholar with the Bradley Department of Electrical and Computer Engineering, Virginia Tech, under the fund of the China Scholarship Council. He is currently a Lecturer with the School of Electrical and Information Engineering, Jiangsu University of Technology. His current research interests include Industrial Internet of Things, Internet of Vehicles, and video caching, computing, and communication.

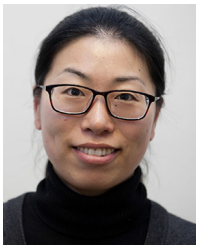

XIAOLI CHU (Senior Member, IEEE) received the B.Eng. degree in electronic and information engineering from Xi'an Jiaotong University in 2001, and the Ph.D. degree in electrical and electronic engineering from the Hong Kong University of Science and Technology, Hong Kong, China, in 2005. She is a Professor with the Department of Electronic and Electrical Engineering, University of Sheffield, U.K. From 2005 to 2012, she was with the Centre for Telecommunications Research, King's College London. She has coauthored over 200 peer-reviewed journal and conference papers, including eight ESI Highly Cited Papers and the IEEE Communications Society 2017 Young Author Best Paper. She coauthored/co-edited the books *Fog-Enabled Intelligent IoT Systems* (Springer, 2020), *Ultra Dense Networks for 5G and Beyond* (Wiley, 2019), *Heterogeneous Cellular Networks—Theory, Simulation and Deployment* (Cambridge University Press, 2013), and *4G Femtocells: Resource Allocation and Interference Management* (Springer, 2013). She received the IEEE COMMUNICATIONS LETTERS Exemplary Editor Award in 2018. She is a Senior Editor of IEEE WIRELESS COMMUNICATIONS LETTERS, an Associate Editor of IEEE TRANSACTIONS ON NETWORK SCIENCE AND ENGINEERING, and an Editor of IEEE OPEN JOURNAL OF VEHICULAR TECHNOLOGY.

PINGZHI FAN (Fellow, IEEE) received the M.Sc. degree in computer science from Southwest Jiaotong University (SWJTU), China, in 1987, and the Ph.D. degree in electronic engineering from Hull University, U.K., in 1994. He is currently a Presidential Professor with SWJTU and an Honorary Dean of the SWJTU–Leeds Joint School, and has been a Visiting Professor with the University of Leeds, U.K., since 1997. He served as a Chief Scientist of the National 973 Plan Project from January 2012 to December 2016. His research interests include high-mobility wireless communications, massive random-access techniques, and signal design and coding. He is a recipient of the U.K. ORS Award in 1992, the National Science Fund for Distinguished Young Scholars (NSFC) in 1998, the IEEE VT Society Jack Neubauer Memorial Award in 2018, the IEEE SP Society SPL Best Paper Award in 2018, the IEEE/CIC ICCC 2020 Best Paper Award, the IEEE WCSP 2022 Best Paper Award, the IEEE ICC 2023 Best Paper Award, and the IEEE VT Society Best Magazine Paper Award in 2023. He served as an EXCOM Member for the IEEE Region 10, IET (IEE) Council, and the IET Asia–Pacific Region. He is an IEEE VTS Distinguished Speaker in 2019–2025 and a Fellow of IET, CIE, and CIC.